AD-A234 903

DTIC

(2)

CUMENTATION PAGE

Form Approved
OMB No. 0704-0188

1	1b. RESTRICTIVE MARKINGS
2a. SECURITY CLASSIFICATION AUTHORITY	3. DISTRIBUTION / AVAILABILITY OF REPORT: Approved for public release, distribution unlimited
2b. DECLASSIFICATION / DOWNGRADING SCHEDULE	
4. PERFORMING ORGANIZATION REPORT NUMBER(S)	5. MONITORING ORGANIZATION REPORT NUMBER(S): AFOSR-TR- 91 0233
6a. NAME OF PERFORMING ORGANIZATION: UNIVERSITY OF CALIFORNIA	6b. OFFICE SYMBOL (If applicable)
7a. NAME OF MONITORING ORGANIZATION: AFOSR AFOSR/NA Bolling AFB DC 20332-6448	
6c. ADDRESS (City, State, and ZIP Code): University of California Berkeley, CA 94720	7b. ADDRESS (City, State, and ZIP Code): AFOSR/NA Bldg 410 Bolling Air Force Base Washington, D.C. 20332
8a. NAME OF FUNDING / SPONSORING ORGANIZATION: AFOSR/NA Bolling AFB DC 20332-6448	8b. OFFICE SYMBOL (If applicable): NA
9 PROCUREMENT INSTRUMENT IDENTIFICATION NUMBER: F-49620-88-C-0131	
8c. ADDRESS (City, State, and ZIP Code): AFOSR/NA Bolling AFB DC 20332-6448	10. SOURCE OF FUNDING NUMBERS

PROGRAM ELEMENT NO.	PROJECT NO.	TASK NO	WORK UNIT ACCESSION NO
61102F	2302	C2	

11. TITLE (Include Security Classification)
Dynamic Energy Absorption of Sandwich Structures by Inelastic Deformation

12. PERSONAL AUTHOR(S)
Professor Werner Goldsmith/Professor Jerome Sackman

13a. TYPE OF REPORT	13b. TIME COVERED	14. DATE OF REPORT (Year, Month, Day)	15. PAGE COUNT
Final	FROM 9/1/88 TO 12/31/90	91/02/05	91

16. SUPPLEMENTARY NOTATION

17. COSATI CODES			18. SUBJECT TERMS (Continue on reverse if necessary and identify by block number)
FIELD	GROUP	SUB-GROUP	Sandwich plates, honeycombs, energy absorption, protective shielding, plastic deformation, impact loading

19. ABSTRACT (Continue on reverse if necessary and identify by block number) An investigation concerned with Inelastic Deformation of Sandwich Plates and Shells under Dynamic Loading consisted of an experimental and an analytical study of the energy absorption capability of honeycomb and honeycomb sandwich structures. Laboratory tests of both types of samples were performed under both static and dynamic loading conditions, the former by means of an MTS testing machine, while the latter involved the firing of a 1.85 lb projectile against the specimens. The targets were attached to a ballistic pendulum arrangement either by a rigid backing or else by means of a simple support. Force-deformation curves were obtained by means of displacement and acceleration transducers. An analysis based on perfectly plastic behavior of the sandwich was obtained that permitted partial integration and hence minimized the computational procedure for the case of the backed sandwich; this was found to be in very good agreement with test results. Aluminum and Nomex honeycombs were employed as cores, while mostly aluminum face plates were employed, although polycarbonate, ABS and fiberglass materials were also investigated.

Energy absorption was found to depend on both the crushing of the honeycomb cores and the deformation of the facings. The limiting practical energy absorption of the target was (over)

20. DISTRIBUTION / AVAILABILITY OF ABSTRACT	21 ABSTRACT SECURITY CLASSIFICATION
☐ UNCLASSIFIED/UNLIMITED ☒ SAME AS RPT ☐ DTIC USERS	UNCLASSIFIED

22a NAME OF RESPONSIBLE INDIVIDUAL	22b TELEPHONE (Include Area Code)	22c OFFICE SYMBOL
DR SPENCER WU	202-767-6962	AFOSR/NA

DD Form 1473, JUN 86 — Previous editions are obsolete. SECURITY CLASSIFICATION OF THIS PAGE

UNCLASSIFIED

19. Abstract (continued)

attained when the core had densified. A condition of punch-through of the face plates, representing shearing of the covers, constitutes a catastrophic failure of the protective device which is to be avoided. The best energy absorption for a given thickness of the sandwich results from a combination of core and facing materials and thicknesses that provide for maximum plastic deformation of the face plates with concomitant total compaction of the core.

FINAL REPORT

on

INELASTIC DEFORMATION OF SANDWICH PLATES AND SHELLS UNDER DYNAMIC LOADIN

for the Period 9/1/88 to 12/31/90

to the Air Force Office of Scientific Research, Bolling Air Force Base,

Contract No. AFOSR F49260-88-CO-0131

Technical Monitor: Dr. Spencer Wu

AFOSR-TR- 91 0233

by

Werner Goldsmith, Principal Investigator
Department of Mechanical Engineering

and

Jerome L. Sackman, Co-Principal Investigator
Department of Civil Engineering

UNIVERSITY OF CALIFORNIA, BERKELEY, 94720

February 15, 1991

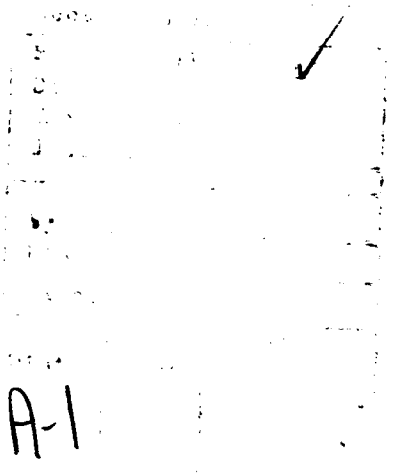

91 4 16 028

FINAL REPORT

on

INELASTIC DEFORMATION OF SANDWICH PLATES AND SHELLS UNDER DYNAMIC LOADIN

for the Period 9/1/88 to 12/31/90

to the Air Force Office of Scientific Research, Bolling Air Force Base,

Contract No. AFOSR F49260-88-CO-0131

Technical Monitor: Dr. Spencer Wu

by

Werner Goldsmith, Principal Investigator
Department of Mechanical Engineering

and

Jerome L. Sackman, Co-Principal Investigator
Department of Civil Engineering

UNIVERSITY OF CALIFORNIA, BERKELEY, 94720

February 15, 1991

INTRODUCTION

This document constitutes the Final Report on Contract AFOSR F49260- 88-0131 entitled "Inelastic Deformation of Sandwich Plates and Shells under Dynamic Loading," with the Air Force Office of Scientific Research, Bolling Air Force Base, Washington, D. C. The work covered the period from 09/01/88 to 12/31/90 and was monitored by Dr. Spencer Wu. The Principal Investigator was Professor Werner Goldsmith, Department of Mechanical Engineering and the Co-Principal Investigator was Professor Jerome L. Sackman, Department of Civil Engineering, University of California, Berkeley.

The project personnel has also included Gregory H. Smyers, who has received the M. S. degrees and Walter Beckmann who will receive this degree shortly; both are currently employed in engineering positions in industry in Berkeley and in the Los Angeles area, respectively. Mr. Beckmann's M.S. research contribution consisted of the static and dynamic response of rigidly backed sandwich plates involving aluminum honeycomb cores; face plates of aluminum, fiberglass, Lexan and ABS were employed.

Approximately half of the results for aluminum face plates are contained in the second Semi-annual Report for this contract dated March 15, 1990; the results for additional configurations tested since that time are included as Appendix A to this report. Furthermore, Mr. Beckmann was awarded the degree of Master of Engineering, the fulfillment of which included a thesis-type report entitled "Dynamic Energy Absorption Characteristics of Edge-Supported Sandwich Plates," which is included as Appendix B. Mr. George Quinones, a Ph. D. student in the Department of Civil

Engineering, has joined the project during the last 3 months; his attention is directed towards obtaining additional experimental information on simply supported sandwich plates and cylindrical sandwich shells.

Mr. Michel Jamjain, a Ph. D. candidate in the Department of Civil Engineering, is concerned with the construction of analytical and numerical models of the impact phenomenon. During the summer of 1990, Brian Duckering temporarily joined the investigation and developed the technique for constructing curved sandwich samples, and Mr. Xiofang Hou as well as other members of the laboratory have assisted in the conduct of a few of the experiments.

Prior to this time, the following documents have been submitted to AFOSR:

1) First Semi-Annual Report, March 15, 1989

2) Highlights of the Achievements (Special Request), September 8, 1989

3) First Annual Report, September 29, 1989

4) Second Semi-Annual Report, March 15, 1990

5) New Proposal entitled "Microstructural and Global Effects in Impacts on Sandwich Plates," May 15, 1990. We were advised in December, 1990 that this proposal could not be funded at this time.

6) Request for No-cost Extension, July 1, 1990.

Included with these documents, and therefore not submitted herewith, were:

A) Ph. D. Qualifying Examination Research Project by Michel Jamjain, "Analysis of the Deformation of Rigid/Plastic Sandwich Plates Supported at the Rear due to Projectile Impact." Included in (4).

B) M. S. Thesis by Gregory H. Smyers entitled "Energy Absorption of Aluminum Honeycomb (11 June, 1990). Included in

(6).

The equipment used for all dynamic tests is shown in Fig. 1. It consists of a massive 2-ton steel table on which all other devices are mounted. This consists of an air gun with a triggering button and a bent from which a massive steel block wwith flat, parallel surfaces was ballistically suspended by means of two wires and on which the samples were mounted either directly, or else simply supported on a brass ring. The projectile consisted of a slightly curved steel head mounted on a circular cyldrical aluminum tube, of 2.85 in. diameter, from which grommets extended for guidance inside the gun barrel. The initial velocity of the striker was measured by a set of parallel laser beams focused onto photocells whose interruption by striker passage produced signals that were recorded by an oscilloscope.

The motion of the projectile was also observed by an eletro-optical transducer that sensed displacement histories which were also recorded on an oscilloscope. An accelerometer was placed on the back side of the block directly behind the impact point whose reading provided meaningful information only for the case of fully backed samples. A rod moving in two sleeves was placed in contact with the rear of the block that indicated the maximuum excursion of the pendulum. The details of the apparatus, the procedure and the data reduction process are described in the reports previously submitted. The body of this final report will concentrate on progress since (4), but will include an overall summary of the results of this investigation.

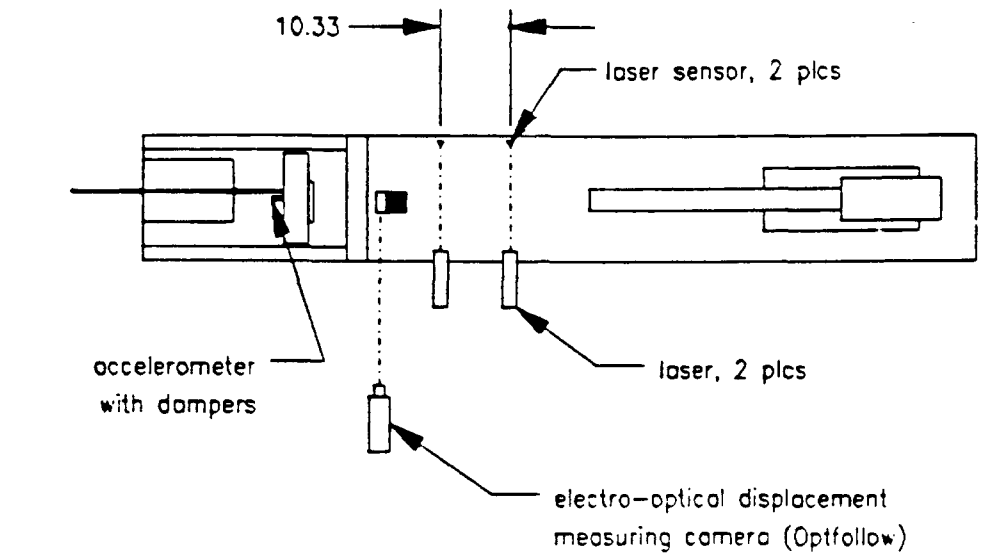

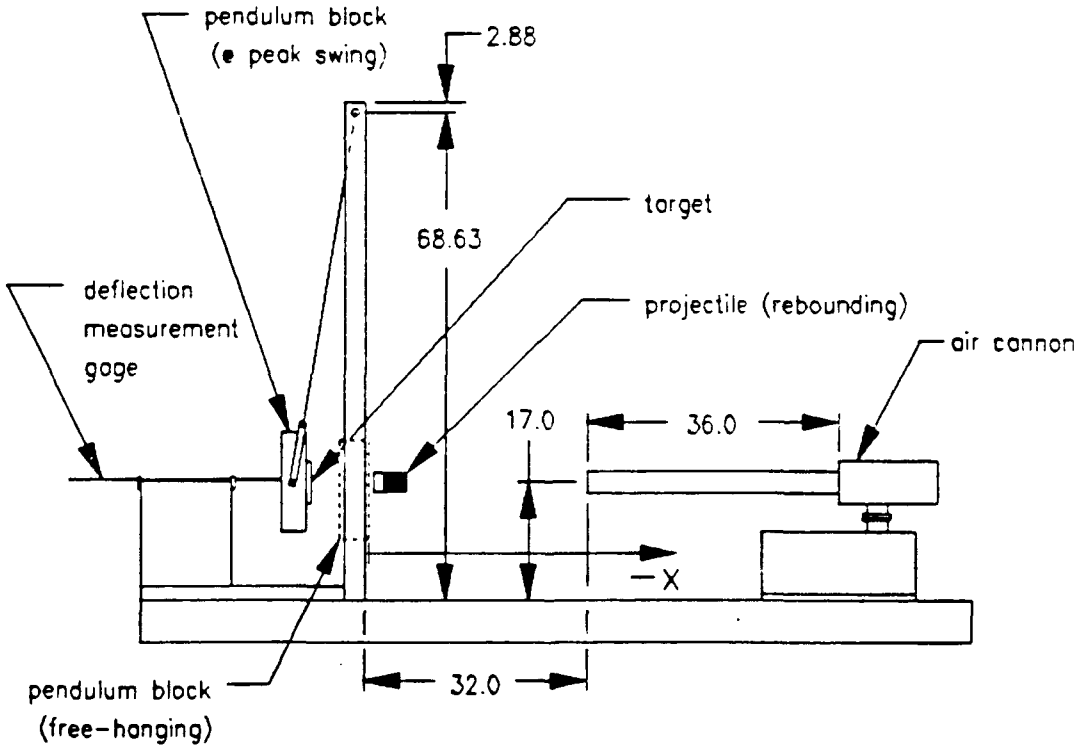

Figure 1

Equipment Configuration:
Dynamic Crush Test

Note:
Dimensions in inches.

CORE MATERIAL

The present investigation was focused on aluminum honeycomb for the core material since a preliminary study indicated that this was the most efficient energy absorption substance of those tested. Nomex (a polymer-treated paper) should also be more closely examined, but this was beyond the scope of the present program.

The material characteristics of the aluminum honeycombs employed and calculated values for the strength are as follows:

TABLE 1

ALUMINUM HONEYCOMB CHARACTERISTICS

Honeycomb Designation[a]	Weight Density lb/ft^3	Crush Strength, psi			
		Published Data[b]	Measured[c]	Measured[d]	Calculated
1/4-.001	2.3	75	81	97	70
F-40-.0019	3.1	165	--	165	--
1/4-.002	4.3	230	233	278	222
1/8-.001	4.5	260	--	274	222
1/8-.002	8.1	750	713	830	706

[a]Honeycomb designation is defined as cell width and wall thickness, both inches.

[b]Hexcel Corp., Dublin, CA, Mechanical Properties of Hexcel Honeycomb Mat TSB 120, 1987.

[c]Specimen diameter the same size as that of the crushing head. Strain r 0.001-0.006 in/s.

[d]Specimen diameter larger than that of the crushing head. Strain rate f 0.001-0.006 in/s.

[e]Predicted by Wierzbicki's formula: $S_m = 16.56\ S_o(t/D)^{5/3}$ where S_o was t 42,000 psi for 5052-H38 aluminum, t is the wall thickness and D is the size. [T. Wierzbicki, "Crushing Analysis of Metal Honeycombs," Int. J. Engng., v. 1, pp. 157-174, 1983.

SUMMARY OF THE RESULTS OF THE INVESTIGATION PRESENTED IN PREVIOUS REPORTS

The objectives of this investigation were the determination of suitable configurations for sandwich plates to serve as dynamic energy absorbers under certain conditions of constraint. The latter were constructed to entail a maximum thickness criterion, chosen here on practical grounds as 1 inch, a peak force transmission limitation characterized by the perfectly-plastic plateau level of various sandwiches for a backed sample, and a capability for maximum energy absorption for unit volume of structure. The fulfillment of these goals were achieved by means of a combined experimental and theoretical investigation.

The initial configuration for which the greatest amount of information has been obtained involved the study of the sandwich behavior when backed by a massive plate. The test results provided a clear indication of the limit of energy absorbed for the backed plate when densification is initiated and the unit becomes saturated. Densification is manifested by a sharp rise in the force-displacement curve corresponding to a direct compression of the material rather than inelastic buckling of cells.

It should also be pointed out that even for the present support condition, the upper plate experiences two different modes of behavior: the first, and presumably the appropriate design paradigm, is a bending and stretching of this component which still permits crushing of the central region of the core, i.e. the contact region and adjacent zones. The second mode is the shearing of the top plate, involving at least some bending of the top plate until punch-through occurs. The analytical effort

of the present study has been confined to the first mode of behavior; a subsequent task should be a modeling of the shear failure condition. However, the present report also incorporates a study of the effect of the accreted mass of the honeycomb in pure compression; this is presented in Appendix C. In addition, a significant amount of data has been collected for a simply-supported circular plate, reported in Appendix B.

The first semi-annual report contained a list and discussion of pertinent references of research related to the current investigation. The reference list is reproduced as Appendix D and is in addition to the extensive bibliography included in the proposal. In addition, the process involved in the selection of candidate core materials, the experimental arrangement for the static and dynamic crush tests, and the procedure for fabricating sandwich specimens were described. Core materials considered included: Solid glass beads alone or in Ecofoam, Styrofoam, Microballoons in foam and in Epoxy. These materials and combinations were not found to be as satisfactory as either aluminum or Nomex honeycombs or other cell geometries.

In particular, aluminum and Nomex (an Aramid (Kevlar) fiber-reinforced phenolic-dipped paper) honeycomb as well as Flexcore configurations, were found to be most useful. Furthermore, they are readily commercially available at reasonable cost, and hence were utilized exclusively in the subsequent investigation. The investigators are grateful to Hexcel Corporation, Dublin, CA, and, in particular, to Mr. Tom Bitzer, for contributing numerous sheets of various sizes and types of cell configurations of the

two core materials employed. Techniques for differentiation of observed displacement histories were described. A typical load-displacement curve was included.

The first annual report provided descriptions of further experimental developments including an improvement of the support structure for the test samples. The results from ten quasi-static and twenty-five dynamic tests on aluminum honeycombs of various cell sizes, geometries, and wall thicknesses were presented. Full crush displacements and the energy absorbed were given as functions of the static peak load. Corresponding dynamic data were provided for the impact of a 1.85 lb circular cylindrical aluminum-steel projectile of 2.88 in diameter. Numerous load-crush curves for both types of loading conditions were provided for which the back of the sample was rigidly supported by a massive plate embodied in a ballistic pendulum arrangement.

One static and several dynamic tests were executed on aluminum sandwich plates, and similar information was obtained. The static crush load for the sandwich composed of two 0.05 in. thick 5052 aluminum face plates and a 1/4-0.001 5052 aluminum hexagonal core 0.75 in thick was found to average 2900 lb, with a peak value of 3600 attained at the point of load removal. The average dynamic crush load for the same sandwich struck by the projectile at a speed of 863 in/s, that produced about the same amount of crush, 0.56 in, corresponding to a 75% value, was found to be 3300 lb, with a peak value of 3790 lb.

Examination of the deformation patterns of the sandwich plates indicated axially-symmetric indentation separated from the undisturbed portion by a annular, plastically-deformed ring.

This ring faired into the unstrained region and exhibited increasing curvature towards the center, with a strong discontinuity in slope occurring at the position corresponding to the radius of the striker. This feature prevailed whenever the striker velocity was sufficiently low to prevent complete densification of the core. When this phenomenon was generated at higher impact velocities, the damage pattern was completely different. Non-axi-symmetric deformation involving buckling of the entire upper face plate was produced whenever the size of the plate was such that interacting wave reflections from the boundaries were sufficiently intense to produce this effect.

The second semi-annual report indicated further improvements in the experimental arrangement and procedure. A comparison of the static and dynamic crush strength of aluminum cores indicated that the dynamic crush strength was 12 to 33 percent higher for 1/8 in. and 1/4 in. hexagonal honeycombs and Flexcore samples with wall thicknesses ranging from 0.001 to 0.002 in. The strain rates for these two types of tests were determined to be 5.7 x 10^{-3} and 6.7 s^{-1}, respectively. Six quasi-static tests to full crush were conducted on sandwich specimens 1/8-001, 1/8-002 and 1/4-001 cores, all 0.75 in. thick; the results are reproduced in Appendix E. These tests produce a condition of punch-through, which result in a partial or full separation of the section of the upper plate under the projectile from the remainder of this sheet.

The data indicate that the energy absorbed at full crush depends on cell size, wall thickness and facing plate thickness;

a smaller cell size and a greater wall thickness results in larger energy absorption, and the trend is the same as the plate thickness is increased. However, the more resistant honeycombs concomitantly exhibit a higher aereal density and thus may be functionally not as useful, albeit capable of absorbing greater amounts of energy. A denser core produces punch-through at a smaller crush. It was noted that sandwich specimens with lowest core density (1/4-001) absorbed four times the energy of corresponding bare core samples; this ratio was 2:1 for 1/8-001 cores and 1.1:1 for the densest sandwich core, 1/8-002 for the same face plate thickness. This is due to the distribution of loading and partial crushing of the region adjacent to the contact zone, as well as the deformation of the face plate. In general, the more material that is plastically deformed for the same percentage of crush, the greater the energy absorption. Similar trends are observed for the energy absorbed just prior to punch-through.

The full crush for sandwiches was found to occur at a smaller deflection than in the case of corresponding cores. An examination of the buckling pattern for sandwiches and bare shows indicated that, for the latter, the entire thickness of the honeycomb buckled, whereas for the sandwich, a region about 0.02 in. long normal to the face plate did not buckle. This is attributed to the stiffening effect of the adhesive employed in the sandwich construction.

The results indicate that participation of the core in the deformation process outside the contact region depends on the interrelation between the density of the core and the face plate thickness. Thus, it is desirable to engage as much core volume

in energy absorption as possible before densification occurs. Too thin a face plate for a core of given density will not transfer sufficient load to the adjacent region to make efficient use of neighboring material. Further, a thin face plate encourages punch-through beyond which the adjacent core is no longer helpful. The ideal situation, that is, the desired design condition for any structural application, is represented by an impact resulting in this catastrophic failure just prior to densification.

On the other hand, face plates with too great a thickness will reduce the crushing process, induce a rebound of the striker and thus raise the level of the transmitted force, an undesirable condition. This is documented by the data which indicates an increase in this average force with plate thickness for a given core. Furthermore, the outer diameter of the plastic zone in the plate facing depends upon core density and plate thickness. For a given core density at full crush, the diameter increases with plate thickness; for a given plate thickness, the diameter increases with decreasing density.

The results from seven dynamic tests on sandwich specimens are also shown in Appendix E together with the pressure-crush curves for these collisions. Cross sections of the samples were examined and the cellular changes were observed; this is crucial because the modeling effort is critically dependent on the mesoscopic deformation pattern of the core. A study of the in terfacial bonding was executed by comparing such deformation and the energy absorption capability of securely and lightly bonded

systems. Upon debonding, an entirely different deformation pattern of the top facing occurred, involving crinkling as well as axially symmetric bending. This behavior is so complex that, at the present time, it appears analytically intractable. Additionally, this type of behavior pattern is definitely not desired because it does not optimally utilize the crush capability of the core. This was demonstrated by a comparison of the crush load-deformation pattern where the well-bonded sample exhibited 50% higher energy absorption prior to punch-through than the weakly bonded specimen; however, the latter still absorbed about twice the energy of a bare honeycomb.

The M. S. thesis of Gregory H. Smyers, submitted with the request for a no-cost extension and entitled "Energy Absorption of Aluminum Honeycomb" is confined to the static and dynamic behavior of this component of the system. In addition to the test data, this document compares the test results with the predictions of simple models generated by others, with good correlation. The results of 26 shots into five different honeycombs show a plateau in the crush force from 10 to 80 percent crush like the plateau in quasi-static tests. For each honeycomb, this plateau is constant over a range of impact velocities and is 27-53 percent higher than the quasi-static plateau. This increase is attributed primarily to the increase yield strength of the material at the high rates of strain in the dynamic tests. Good agreement between different shots into the same honeycomb and between the data from different transducers in the same shot strongly supports the accuracy of the results.

As an additional comment on the data presented in the pre-

vious and present report, it is evident that the number of variables that significantly affect the response of the system is so large that a complete experimental examination of their effects is prohibitive. In consequence, the construction of a realistic, yet tractable analytic model that can provide a clear picture of the interrelationships between these parameters and the response of the structure to impact is imperative for optimal design. Such an initial model, which was transmitted with that report and is described below, constitutes a first step in the fulfillment of this goal.

An analytical representation of the global deformation of the backed sandwich structure was developed by Michel Jamjain as part of his doctoral requirements. The model involved a rigid-plastic face plate and honeycomb backed by a rigid foundation, and the principles of momentum conservation of continuum mechanics and the yield condition based on laboratory measurements were employed to get an analytical formulation consisting of a set of system of integro-differential equations after execution of a partial closed-form integration of the relations. The final result had to be obtained by numerical integration, but without spatial discretization. The final computed information, consisting of the radius of the affected area of the top plate, the projectile velocity and the central plate displacement, all as function of time, as well as the final deflection of the target as a function of the radius, was compared with experimental results and found to be in very good correlation for a number of representative experimental conditions.

ACCOMPLISHMENTS DURING THE PERIOD 02/28/90 TO 12/31/90

A substantial portion of the effort during this interval was devoted to:

(1) The static and dynamic testing of sandwich plates backed by a rigid block, particularly for facings other than aluminum, i.e. ABS, fiberglass and Lexan, involving three different aluminum cores;

(2) Further data acquisition, particularly with respect to the testing of simply-supported sandwich plates;

(3) The modelling and study of the effects of mass accretion of crushed honeycomb material on plate behavior;

(4) The correlation of experimental results with predictions of the honeycomb response formulated both here and, empirically, by others;

(5) The correlation of analysis and experiments for the tests on backed sandwich plates;

(6) The initiation of a predictive model corresponding to impact on simply-supported sandwich plates;

(7) The development and implementation of a technique for constructing honeycomb shells, as well as preliminary testing, and

(8) The compilation, description and publication of the work accomplished under the present contract.

(1) A series of 6 static and 19 dynamic tests of sandwich plates with several types of aluminum honeycomb with aluminum, Fiberglass, Lexan (polycarbonate) and ABS were conducted with the test matrix and results included in Appendix A. The data reduction process for this set of results was initially executed using accelerometer information for determining the force or pressure and results recorded by the electro-optical displacement transducer (OPTFOLLOW) for the displacement or crush.

A plot of the resulting pressure/crush curve exhibited anomalies in the region of maximum deformation that was believed

to be due to irregularities associated with the accelerometer record. In order to overcome this problem, the displacement data was fit by a multipolynomial spline and then doubly differentiated to produce an acceleration history of the projectile from which the force history was deduced. This appeared to cure the problem; however, it was discovered that the form of the acceleration curve was highly dependent on the degree of the polynomial. When a higher-order spline was used, the anomaly, in the form of curve looping, reappeared. Thus, higher-order spline fits were avoided; alternatively, smoothed accelerometer could have been used for the force histories.

In view of the diverse materials and thicknesses of the covers and the cell size and wall thicknesses of the aluminum honeycomb, the dynamic energy absorption data presented in Appendices A and E are most conveniently compared on the basis of energy absorbed per percentage of crush. Examination of the data reveals that for identical cores, a thicker face plate provides a higher absorption capacity for the same degree of core deformation, as indicated by comparison of Runs 17I, 18I and of 6I, 7I.

On the other hand, the degree of crushing produced also controls the relative energy absorption per unit crush in that the energy absorbed by the face plate is engaged to a greater extent, the greater the crush, and this depends entirely on the impact velocity for a given striker. This is most strongly documented by comparing the data from Runs 3H (or 6H) with Run 5H and 4H, where the increase in total absorbed energy is much greater than the ratio of the corresponding impact velocities. It is also supported by the results of Runs 10I and 14I and Runs

5I and 8I for fiberglass, respectively, and also for Runs 7I and 12I with Lexan, as well for Runs 4I and 11I for ABS face plates. These results must additionally be gaged in the light of whether punch-through occurred, i.e., either partial or complete separation of the region of the face plate directly below the striker from the remainder of the surface. In such a case, energy is absorbed by shearing that is not included in the reported amount of the absorbed energy. For aluminum, the energy for a complete separation of the plug is estimated to be between 5 and 10 percent of the total energy absorbed.

Inspection of the data from the various portions of this investigation provides some insight into the effect of core density on unit energy absorption. The results for the tests on 1/8-.001 honeycomb with either 0.0032 or 0.0050 in. thick face plates listed in Table 2 of Appendix E all exhibited some degree of punch-through, with the heavier core inducing complete detachment of the impact region of the top face plate from the remainder of that body. This is demonstrated by a comparison of the data for a 1/8-0.001 (Run 3D) and 1/8-0.002 core with the same face plate thickness of 0.050 in. (Run 5D). The impact velocity for the lighter core was about 33% lower (953 in/s) than the heavier core (1,347 in/s), while the energy absorbed per percent of crush for the former (44.0 in-lb/%) was also lower than that for the denser material (68.2 in-lb/%) by approximately the same percentage.

Comparison of results from both Appendix A, Run 17I (1/8-.002, 0.050 aluminum face plate, initial velocity 1,233 in/s)

and Appendix E, Run 7D (1/8-.001, 0.050 aluminum face plate, initial velocity 1,113 in/s) shows the energy absorbed per percent crush to be 54.6 and 41.5 in-lb/%, respectively. This further documents the high degree of nonlinearity of the system behavior as well as the influence of the core density on energy absorption. Clearly, the most effective protection is provided when the core has virtually attained the state of densification.

The same conclusion is reached when the data for 0.0385 in thick Lexan face plates is examined in Table 2 of Appendix A where no punch-through occurred. Run 6I has 1/8-.001 core with a weight density of 4.5 lb/ft^3 and features a velocity of 757 in/s, while Run 9I with a F40-.0019 core (with a weight density of 3.1 lb/ft^3) involves an impact speed of 715 in/s. The former absorbs 22.1 in-lb/%, while the latter absorbs 14.4 in-lb/%.

A complete investigation of the effect of striker shape, mass and material is highly desirable, but was well beyond the financial and time constraints of the present investigation. Furthermore, not surprisingly, all other things being equal, aluminum face plates provided a greater degree of energy absorption per unit crush than the other materials investigated, due to the higher yield strength of the aluminum.

In comparing the effectiveness of the facing material, it is evident that aluminum, the only metal tested, provides for greater energy absorption than any of the nonmetallic materials employed in the investigation, as manifested by the permanent deformation of the face plates. With other materials, different deformation patterns were observed. In one case, an impacted Lexan facing fractured through the plate in an irregular line

Lexan facing fractured through the plate in an irregular line away from the contact area, and the smaller region of the top face was totally debonded. In addition, the circumference of the indenter sheared a plug of the plate with its crushed honeycomb below; however, the deformation of the circular ring around this indentation experienced an elastic rebound that caused debonding from the partially crushed core. A similar behavior was experienced with Fiberglass, except that the debonded annulus around the crater was substantially smaller. With an ABS impact face, the annulus around the crater was plastically deformed and no significant elastic rebound was observed, i.e. the crushed core in the annulus around the crater remained bonded to the face plate.

(2) The M. Eng. thesis of Walter Beckmann, entitled "Dynamic Energy Absorption Characteristics of Edge-Supported Sandwich Plates," submitted July 26, 1990, and included with this Final Report as Appendix B, contains all of the results obtained for the case of the simply-supported sandwich plates whose impact response was quite different from that of such backed plates. In all but one case, crush-through did not occur; here, the major damage mechanisms were the plastic deformation of the top and bottom plates (with the latter somewhat less than the former) and far less crushing of the core than found in the case of supported plates. However, a shear banding was found in virtually all samples, whose extent in some cases was localized around the edge of the crater, such as shown in Fig. 15 of Appendix B, while in others (such as Run 5 of Table 1 of Appendix B), the banding

extended over the entire diametral section.

In still other cases (Run 8 of Table 1), this banding is evident over nearly the entire cross section, but is diminished successively in extent over the core depth beyond a critical radius and disappears completely within a short distance from the edge. Concomitantly, the amount of crush is very substantially reduced over the corresponding backed samples struck at similar velocities because the rigidity of the rear plate generated tubular buckling; this resistance from the back surface was substantially minimized in the present configuration. Thus, the partition of absorbed energy is shifted towards face plate deformation, with the effect on the core substantially minimized. It must be emphasized that this situation prevails only when punch-through does not occur; should this situation prevail, the damage pattern is expected to be similar to that of backed plates, but will occur at much higher impact energies. In this regime, only one test was executed; it is obvious that additional experimentation should be conducted and correlated with an analytical model of this structure which has, as yet, not been developed.

(3) The process of compression of backed sandwich plates occurred by local buckling of the honeycomb cells under the projectile and in outer, adjacent region where the plate deflects. This event simulates an accordion formation whose extent in the direction of the cell axis depends upon the initial velocity of the striker, i.e., complete crush or densification corresponds to accordion buckling over the entire core depth. This accumulating mass is driven by the entry of the striker, and its inertia contributes to the deceleration of the striker. In

the initial analysis for the backed sandwich structure, this effect had not been taken into account. Appendix C provides an evaluation of the effect of this mass by including additional terms in the governing equations of the backed plate analysis that was submitted as part of item (4) of the previously submitted material.

The honeycomb was modeled as a continuum with varying density resulting from the mass accretion; the face plate was assumed to be rigid/plastic. This analytical model also required a numerical solution effected finite difference techniques. It was found that the inclusion of this accreting mass was absolutely negligible in the calculation of the central deflection, time of contact, rebound velocity and terminal location of the boundary of the plastic zone. It must be emphasized, however, that this conclusion pertains only to the range of parameters studied which corresponded to those employed in the experimental matrix.

(4) The M.S. thesis of Gregory H. Smyers, previously submitted as indicated in item (6), concentrated on the static and dynamic behavior of the honeycomb alone. Most of the experimental results obtained in the present investigation have been detailed in previous reports. However, both the writing of the thesis and, in particular, the comparison of certain experimental results with expressions found in the literature have been accomplished since the date of the second semi-annual report.

The static crush strength of aluminum honeycombs is presented in Table 1; the agreement between the present measured values of samples of the same size and the predictions using the expression

developed by Wierzbicki is excellent. It may be noted that the crush strength data for oversize samples is significantly higher; this is attributed to the constraining effect of the surrounding, unloaded material. The current measurements agree with the published data of the manufacturer to better than 10%.

The significant increase of the dynamic crush strength relative to the static values was shown in the thesis accompanying (6) to be not due to either accreted mass or trapped air in the cells and is probably due to the strain rate dependence of the material.

As a final comparison with published empirical expressions, the folded half-length of the buckles in aluminum honeycombs due to static and dynamic loading will be examined. The computed and experimental results are presented in Table 2. It may be observed that (a) the dynamic data are consistently higher than the static values, but by only a very small amount, and (b) the theoretical values are very near the measured information.

TABLE 2

FOLD HALF-LENGTH IN FULLY CRUSHED ALUMINUM HONEYCOMB SPECIMENS

Honeycomb Designation	FOLD HALF LENGTH[1] Quasi-Static Crush Measured[2]	Theoretical[3]	Dynamic Crush Measured[2]
1/4-.001-2.3	0.023	0.023	0.027
1/4-.002-4.3	0.027	0.029	0.029
1/8-.001-4.5	0.014	0.014	0.015
1/8-.002-8.1	0.020	0.018	0.021

[1] See Fig. 1-3 in the thesis by Smyers for the definition of the fold half-length, H.

[2] Calculated by dividing the original specimen thickness, 0.75 in., by twice the number of folds.

[3] Calculated from $H = 0.569(tD^2)^{1/3}$ [See Note e of Table 1].

(5) The predictions of the analysis both including and excluding the effect of accreting mass, constituting a portion of the doctoral dissertation of Michel Jamjian, is presented in Appendix C. The results when this mass effect is taken into account have been compared to seven experimental runs, as opposed to but a single run in the material previously submitted. Inspection of the results in Table 3 indicates excellent correspondence of calculated and measured extents of the plastic zone and very good correlation for the central deflection of the sandwich structure. The agreement between the predicted and observed values for the contact are not nearly as good; this is attributed to the extreme difficulty in measuring the actual contact time. The analysis is an ingenious application of rigid/plastic theory; it results in a relatively simple of integro-differential equations whose solution by numerical is straight-forward and efficient. At this point, a finite element model of the system has not been accomplished because an appropriate element of the honeycomb has not yet been developed.

While this analysis is highly satisfactory for the backed sandwich plate, it is, of course, inapplicable for a simply supported sandwich structure. The analysis of such a system is still far from complete, and should be vigorously pursued, since this condition is one of very frequent application of a protective shield.

(6) Subsequent to the conclusion of the development of a model for the backed sandwich plate subjected to normal impact by a blunt striker with a diameter large compared to the plate thickness, an attempt was made to extend a similar representation to

the case of a similar simply-supported target. These two conditions represent the majority of the practical cases where shielding of humans or equipment is required. The analysis for either a simply-supported or free plate must, of necessity, include the deformation of the rear facing which was omitted in the case of the backed system. This, then, requires a characterization of the force transmission mechanism in the core, which, after the expenditure of considerable effort, was found to be a very formidable undertaking.

The first attempt to quantify the impact behavior consisted of a modeling of each tubular component as a rigid/plastic element with no direct interaction between adjacent members. When this concept was developed mathematically, it was found that there was a missing condition, that did not could not be incorporated from the usual initial and boundary conditions. Specifically, the position of the inflection point of the deformed facings could not be located except by arbitrary assignment. In terms of the analysis, this position corresponds to a corner of the Tresca yield surface which was employed in the present model, and a corresponding indeterminacy arises with the von Mises yield criterion.

In consequence, two different approaches are being pursued and are currently in their very initial stages. On one hand, a phenomenological model is being considered that replaces the disjointed tube model for the core by an elastic/plastic continuum capable of transmitting only normal forces and transverse shear (similar to a Pasternak foundation). This

technique appears to offer considerable promise, but insufficient time has been able to be devoted to this topic in order to give a reasonable assurance of its successful pursuit.

The other procedure, undertaken concurrently, is a direct numerical evaluation of the system using a finite element method. The key problem in this approach is the development of an appropriate element that will incorporate all the desired force and deformation characteristics required for a reasonable representation of the core behavior. No such element is currently available; it must be formulated from basic principles and tested before it can be implemented as part of an overall program suitable for modeling the response of the composite plate to impact.

Both of the techniques suggested above must be capable of handling the varied comportment of the core at the meso-mechanical level. Experiments indicate that this behavior is substantially more complicated than in the case of a backed sandwich plate. In particular, the coupled effects of facing material and thickness, the core density , material and possibly geometry, as well as the impact velocity activate various mechanism of damage, with certain types of deformations not found in the case of the backed target. As an example, the prominent shear banding, which was highly localized in the backed sample was often found to extend over virtually the entire cross-section of the core.

It should be recalled that the total thickness of all sandwich specimens was maintained constant or nearly so throughout the sequence by design. Variations of this parameter will obviously

increase any test matrix by an order of magnitude. However, within the parameters of the present test sequence, the simply-supported plates exhibited substantially less core crushing and concomitantly plastic deformation which extended over a wider radius of the facing material. This is documented by Table 1 of Appendix B except for Run 3, where punch-through occurred.

(7) A procedure has been developed for the construction of semicircular cylindrical sandwich shells which uses a mold composed of a male and female die with diameters corresponding to the inner and outer dimension of the desired specimen. The sandwiched material should be capable of elastic deformation in a single curvature deflection, rather than a plastic distortion in order to permit maximum energy absorption under impact conditions. This requires employment of a Flexcore layer with a cell shape which permits ready distention without excess of the yield limit anywhere, and, conversely, a return to a plane condi-tion upon removal of the constraint. The core is attached to cylindrically-shaped facings of aluminum and nonmetals over the entire outer and inner surface by a cementing agent. Several such specimens have been manufactured and are ready for testing.

(8) The assembly of the results, analysis of the data, and comparison of the various deformation mechanisms as well as their causes (when evident) have consumed a significant amount of time and effort. The writing of the present report based on this information and incorporation of previously obtained results has also required the expenditure of substantial labor. Within the next several months, the work performed under this contract will

be converted into manuscripts to be submitted to an archive journal, probably either the International Journal of Impact Engineering, the International Journal of Mechanical Sciences, or the International Journal of Solids and Structures. There will be at least two, and possibly three papers generated from the work performed this far. Any additional results to be obtained through further effort on this general program, if support can be generated, will also be converted into a similar archive journal publication.

It should also be mentioned that a reasonable amount of work was spent in supplying part of the documentation listed at the beginning of this report. Specifically, this included items (5) and (6) which were previously submitted.

CONCLUSIONS

A comprehensive investigation of the energy absorption of sandwich plates has been undertaken for a period of approximately 27 months. The program consisted of concurrent experimental, analytical and numerical approaches. At the beginning, a complete search of the literature and an evaluation of pertinent references was performed. Subsequently, a sound procedure for the acquisition of requisite test information, i.e., the complete experimental and measurement technique, was developed and refined in the process of gathering the actual data. After a variety of preliminary experiments, it was concluded that the most promising core material consisted of cellular components, represent here by either aluminum or Nomex honeycombs. Facings of several materials and thicknesses, such as 5052 aluminum,

polycarbonate, Fiberglass and ABS were utilized for the manufacture of the test specimens by cementing these sheets to the cores. In order to restrict the number of parameters affecting the event to somewhat manageable proportions, it was decided to maintain the overall thickness of the composite sample at approximately the same value. This corresponds to keeping the areal density of a protective shield within a reasonably narrow range. Such a restriction is also very likely to be encountered in the requirement for any practical application.

A ballistic test stand was employed that featured an air gun with an approximately 3 in. diameter bolted to a 2 ton steel table. A projectile consisting of a slightly curved steel head attached to a hollow circular cylindrical aluminum body, with a weight of 1.85 lb and a diameter of 2.85 in., was fired normally against the targets at speed ranging from about 400-1500 in/s. The projectile was equipped with rubber grommets serving as runners within the gun barrel, and was painted so that a vertical boundary was formed between a black and a white region. This was effected in order to permit tracking of the motion of the projectile by an electro-optical displacement transducer (OPTFOLLOW 7000 C) that permitted digitizing and subsequent processing of the data.

Targets were attached to a heavy steel block suspended ballistically from a structural bent in either of two modes: (1) Initially square cores and subsequently sandwich plates of the same shape, a approximately 7.5 in. on a side, were centrally and directly positioned on this block so as to provide a completely unyielding backing, but permitting rigid-body motion as the

result of pendulum excursion, and (2) Circular target plates of 11 in., which were simply supported on a brass ring of 10 in. were bolted centrally to the pendulum block. An accelerometer was attached to the center of the back surface of the pendulum block to approximately record the behavior of the backed target only. In the case of the simply-supported sandwich plate, the acceleration record bore no relation to the force history experienced by the frontal sample. In addition a sleeved rod was placed on the support table that touched the rear of the block and was moved to the position of maximum excursion. Measurements were made subsequent to all tests to ascertain the deformation and other damage of the specimen, including post-mortem diametral sectioning.

Concurrently, static testing of samples of cores involving both circular shapes of the same and oversized diameter as the loading head, which was the striker used in the dynamic tests, was executed. In addition, similar tests involving square cores and sandwiches, the same size as used in the dynamic tests were, performed. These were performed on a standard MTS machine in a displacement-controlled mode.

The resulting damage patterns exhibited many and diverse patterns, controlled by the facing material and thickness, the core density and the impact velocity for this series of tests where the striker was always the same and the thickness of the target was nearly the same. The velocity range employed here was intended to permit the advent but not the excess of densification. Distinct differences in behavior were absorbed for the

backed as opposed to the simply-supported target condition. In the former, significant core crush was found whenever the top facing was deformed to the point or very close to the condition of punch-through. Damage was primarily confined to the region below or immediately adjacent to the contact circle of the striker where it was severe. In contrast, for simply-supported plates, a plastic shear buckling was manifested not only in the vicinity of the contact area, but extending further outward, in some cases to the exterior periphery. Clearly the damage mechanism between these two situations are quite disparate.

The results were employed to calculate the amount of energy absorbed in each experiment and to obtain the energy consumed per unit of crush, believed to be the best correlator of the damage in view of the multitude of physical parameters that have a significant influence on the deformation characteristics of the composite target. From the data obtained, it appears as though the best combination for energy absorption consists of as dense an aluminum core as practical coupled with aluminum facings of maximum practical thickness, although this will not represent a condition of minimum areal density. However, use of such combinations of metallic components will permit the design of the level of the peak force that is transmitted to the object being shielded before densification. In most applications, a backed plate situation will prevail, even though the object being shielded may deform more than the pendulum block employed in the present tests. Thus, the use of a rear facing for the protective shield will be necessary in the case of continuous contact with that object if it will prevent

excess deformation by its absence; it does not contribute significantly to the energy absorption.

In contrast, the simply-supported sandwich plate will find fewer applications. Its smaller overall deformation for similar impact energies (using the same projectile) will not involve a danger to the shielded object over the majority of its exposed surface. However, the force transmitted at the simple support is clearly greater than that transmitted over a unit area of the backed-sandwich-plate system, and hence may require additional limiting mechanisms to reduce the transmitted force to specified levels. This aspect, as well as numerous other very interesting facets of the behavior pattern (such as the employment of foams, or the combination of honeycombs cores partially or completely filled with foams; variations of striker mass and geometry; other plate support conditions; influence of lateral boundaries on the deformation pattern; a broader range of impact velocities; a more detailed analysis of bonding effectiveness -- this was brought out only in a few cases where attachment was deliberately weakened -- etc.) could not be explored in the present investigation due to the time and financial constraints imposed.

A complete analysis of striker impact on a backed, metallic, sandwich plate with honeycomb core was executed using rigid/plastic theory and a simplified model of the core that avoids interaction between cells and neglects transverse shear between facing and core. The integro-differential equations resulting from such modeling permitted reduction of the dimensionality of the system providing a system of ordinary differential equations

that was solved numerically. The predictions of this analysis were in very good accord with corresponding experimental results. A refinement of this representation that included the effect of accreted core mass underneath the striker during indentation, that involved an unexpectedly difficult solution procedure, indicated that the effect of this mass is negligible.

The present program had been proposed for a period of three years with a correspondingly larger budget. It was expected that such a time span would permit the execution not only of the work accomplished as indicated in this and previous reports, but would also allow the execution of some additional tests on sandwich plates featuring Nomex honeycombs as the core, a somewhat wider initial velocity range for the tests, and a completed test program for the shells. In addition, the analysis for the simply-supported plate could have been completed, and procedures for the representation of the impact phenomenon on sandwich shells could have been initiated. However, these areas could not be covered due to the financial and temporal constraints imposed.

Nevertheless, the accomplishments of this program funded for 24 months are substantial, due in large measure to the efforts of all participants who devoted far more than their compensated time to the project. This research provides the first hard data on the behavior of a class of sandwich plates under impact that is available in the public domain. Deformation patterns for two types of support conditions have been delineated and contrasted. The limits of utility of energy absorption for these sandwich structures have been obtained for various combinations of facings and cores. The relative benefit of a number of dif-

ferent sandwich compositions have been detailed. It has been shown that substantial additional research is required for a full understanding of the deformation patterns of various structural composites, particularly at the meso-mechanical level. The general subject should be explored further in a directed manner, with particular emphasis on the behavior of practical shields for commercial and military applications.

APPENDIX A

TABLE 1

RESULTS OF ADDITIONAL QUASI-STATIC TESTS ON BACKED SANDWICH SPECIMENS

Original Core Thickness of the 5052 Aluminum Hexcel : 0.75 in

Run No.	Composition			Full Crush Conditions[3]				
	Core	Face Plate Thickness, in	Face Plate Material	Displacement, in[1]	%[2]	Avg. Press. psi	Energy Absorbed in-lb	Energy Absorbed per % of crush in-lb/%
70	F40-.0019	0.0385	Lexan	0.595	79.3	365	1,480	18.7
71	F40-.0019	0.030	Fiberglass	0.500	66.7	250	810	12.1
72	1/8-.001	0.0385	Lexan	0.550	73.3	505	1,760	24.0
73	1/8-.001	0.0335	Lexan	0.535	71.3	410	1,370	19.2
74	1/8-.001	0.060	ABS	0.540	72.0	345	1,120	15.6
75	1/8-.001	0.030	Fiberglass	0.525	70.0	355	1,150	16.4

Run No.	Punch Initiation
70	No
71	Yes
72	Yes
73	Yes
74	No
75	Yes

[1] "Full" crush represents the condition where load-displacement curve rises denoting densification (does not occur at the same displacement as for cores alone).
[2] % thickness decrease = (change in thickness)/(original core thickness) x 100
[3] All tests were carried out to densification.

TABLE 2

ADDITIONAL DYNAMIC TEST RESULTS ON BACKED SANDWICH SPECIMENS
Original Core Thickness of the 5052 Aluminum Hexcel: 0.75 in

Run No.	Composition Core	Face Plate Thickness in	Material	Velocity, in/s Impact	Rebound	Crush[1] Press. psi	Depth in.	Depth %
3H	1/8-.001	0.032	Aluminum	785	--	1168	0.33	44
4H	1/8-.001	0.032	Aluminum	1,054	--	843	0.62	83
5H	1/8-.001	0.032	Aluminum	886	--	1109	0.38	53
6H	1/8-.001	0.032	Aluminum	787	--	1024	0.33	44
4I	1/8-.001	0.060	ABS	747	--	676	0.49	65
5I	1/8-.001	0.030	Fiberglass	464	--	552	0.24	32
6I	1/8-.001	0.0385	Lexan	757	--	736	0.39	52
7I	1/8-.001	0.0335	Lexan	704	--	761	0.37	49
8I	1/8-.001	0.030	Fiberglass	804	--	758	0.49	65
9I	F40-.0019	0.0385	Lexan	715	--	463	0.65	86
10I	F40-.0019	0.030	Fiberglass	474	--	341	0.35	47
11I	1/8-.001	0.060	ABS	796	--	698	0.50	67
12I	1/8-.001	0.0335	Lexan	765	--	807	0.38	50
13I	1/8-.001	0.0385	Lexan	698	--	748	0.33	44
14I	F40-.0019	0.030	Fiberglass	692	--	618	0.40	53
15I	F40-.0019	0.0385	Lexan	494	--	534	0.26	35
16I	F40-.0019	0.0385	Lexan	695	--	506	0.57	76
17I	1/8-.002	0.050	Aluminum	1,233	--	2,111	0.36	48
18I	1/8-.002	0.032	Aluminum	1,234	--	1,815	0.51	68

Run No.	Energy Absorbed, in-lb Total	Per Inch of Crush	Per % of Crush	Punch Initiation
3H	1,184	3,588	26.9	No
4H	2,371	3,824	28.6	Yes
5H	1,577	4,150	29.8	--
6H	1,202	3,642	27.3	--
4I	1,185	2,418	18.2	Yes
5I	403	1,679	12.6	No
6I	1,149	2,946	22.1	Yes
7I	1,024	2,768	20.9	No
8I	1,419	2,896	21.8	Yes
9I	1,235	1,900	14.4	--
10I	481	1,374	10.2	--
11I	1,371	2,742	20.5	Yes
12I	1,197	3,150	23.9	--
13I	966	3,018	22.6	No
14I	1,023	2,415	18.2	Yes
15I	514	1,977	14.7	Yes
16I	1,196	2,098	15.7	Yes
17I	2,621	7,281	54.6	Yes
18I	3,065	6.010	45.1	Yes

[1] Crush = (change in thickness of sample)/(initial core thickness) x 100

APPENDIX B

Dynamic Energy Absorption Characteristics of Edge-Supported Sandwich Plates

Walter Beckmann

Submitted in partial satisfaction of the requirements
for the degree of

MASTER OF ENGINEERING

in the

Graduate Division

of the

University of California, Berkeley

Berkeley, CA July 26, 1990

Dynamic Energy Absorption Characteristics of Edge-Supported Sandwich Plates

by
Walter Beckmann

Abstract

The ability of a protective barrier to absorb kinetic energy in a collision is indicated by the force required to crush it and the extent to which it will crush. To investigate the protection potential of edge-supported aluminum honeycomb sandwich plates, a system was used for measuring the force applied to a cushioning material when it is rapidly crushed, as in a collision. A blunt projectile the size of a soda can is shot into a specimen supported on a circular cylindrical ring mounted on a massive pendulum. Various measurement systems record the motions of the projectile and the pendulum, from which the crushing force as a function of crush depth is determined.

The results for 10 shots into 7 different sandwich configurations show that less dense cores and thinner aluminum face plates make more efficient energy absorbers providing that their energy absorbing capacity is not exceeded. Comparisons to back-supported tests show that edge-supported specimens are much more efficient energy absorbers in that they absorb the same energy at lower crush pressures, due in part to the fact that they make use of the additional energy-absorbing deformation mode of bending of the sandwich as a whole.

Acknowledgments

I thank Professor Werner Goldsmith for his enthusiasm, support, and direction during the course of this research and Professor Jerome Sackman for his insight and ideas.

I thank my laboratory partner, Gregory Smyers, whose ideas, experience and teamwork contributed much to this research. I also thank the other members of the Impact Laboratory for their generous help with laboratory equipment.

I thank Tom Bitzer and his employer, Hexcel Corporation for donating the honeycomb core materials tested, and for help in bonding sandwich plates. I hope this research is beneficial to them.

This research was funded in part by the National Science Foundation (NSF Grant MSM-8800400) and in part by the Air Force Office of Scientific Research (contract AFOSR F49260-88-CO-0131).

Table of Contents

	Page
Abstract	ii
Acknowledgments	iii
Introduction	1
Test Set Up	2
Targets	5
Dynamic Test Results	6
Quasi-Static Test Results	10
Discussion of Test Results	11
Conclusion	22
References	24
Table	25
Figures	26

Dynamic Energy Absorption Characteristics of Edge-Supported Sandwich Plates

Introduction

An experimental investigation has been performed into the behavior of sandwich structures under dynamic loading for the purpose of determining energy absorption characteristics. The investigation began by testing specimens which were supported by a rigid backplate (back-supported). First, back-supported bare honeycomb specimens (with no face plates) were tested. The results of this intial investigation are found in [1]. Next, the investigation advanced to sandwiches. The honeycomb sandwiches were formed by bonding a 0.75 inch thick aluminum honeycomb core between face plates which varied from 0.030 to 0.060 inch thick. Four different kinds of honeycomb cores and five different kinds of face plates were used to form the sandwich specimens. The results of these back-supported honeycomb sandwich tests are reported in [2]. The experimental investigation into back-supported tests has essentially been completed.

Although the data obtained from back-supported tests is quite useful, boundary conditions for actual applications of honeycomb sandwiches as energy absorbers may be quite different. In many practical utilizations, the honeycomb sandwich will surround something fragile to protect it from

damage, and will not be supported by a rigid back plate. In locations such as the sides of a vehicle or the walls of a building, honeycomb sandwich panels may be set into a framework to form a barrier to protect fragile equipment or human beings from impact damage. In such an application, the sandwich encounters boundary conditions much closer to edge-supported than to back-supported. Hence, the investigation has advanced to a consideration of edge-supported boundary conditions. Edge-supported tests to determine the energy absorption characteristics of flat honeycomb sandwich plates have been performed and analyzed. Specimens tested with edge-supported boundary conditions have the advantage over back-supported specimens in that all components of the sandwich are free to bend. The back-supported tests previously done included the deformation modes of axial buckling and shear of the honeycomb core, as well as shear and bending of the face plates. With tests of edge-supported specimens, all of the back-supported deformation modes are possible, plus the sandwich as a whole can bend. No longer is the back face plate held rigid, but it is free to move during crush, allowing bending of all components of the sandwich to occur.

Test Setup

The setup for the edge-supported tests is essentially the same as that for the back-supported experiments. The system designed for investigating high speed crushing of

back-supported specimens is shown in Figure 1. Basically, an air cannon fires a blunt projectile into a target specimen attached to the vertical face of a ballistic pendulum. The projectile is an aluminum tube 2.88 inches in diameter, bonded and pinned to a steel head. The steel head has a slight convex curvature (18-in. spherical radius) to minimize the effect of a slightly "cocked" impact. Before, during and after the impact, various instruments (two lasers with sensors, an Optfollow camera, an accelerometer and a deflection measurment gage) are used to measure the motion of the projectile and of the pendulum. The velocity of the projectile before impact is obtained from the measured time for the interruption of two parallel laser beams spaced 10.33 inches apart. The breaking of the laser beams by the projectile is also used as the trigger for the Nicolet oscilloscope to start recording data. The Optfollow 7000 optical tracking system, manufactured by Ya-Man Ltd. of Tokyo, which is used to measure the linear motion of the projectile during impact, works by "following" a vertical black/white border on the projectile as it passes in front of the camera and through its field of view (FOV). The voltage output by the system varies according to the position of the border in the FOV. An Endevco 2235C piezoelectric accelerometer is attached to the back side of the pendulum as shown in Figure 1 and puts out a voltage that is proportional to the acceleration of the pendulum. The total horizontal deflection of the pendulum is measured

using the deflection gage. From this information, the force-crush relation can be derived. A detailed description of the test set up is contained in [1].

For edge-supported tests, the pendulum was modified by securing a circular cylindrical ring to its front surface to provide edge-support for the targets. Thus, the ring is placed between the target specimen and the pendulum. Four brackets were attached to the outside edge of the ring and bolted to the pendulum, holding the ring flush against the surface of the pendulum. The ring has an inner diameter of 10.0 in, a thickness of 0.15 in, a depth of 1.5 in, and is made of bronze. The size of the ring was chosen to be as large as possible, consistent with the limitation of the size of the pendulum, so that bending of the sandwich as a whole would not require excessive projectile velocity. After attaching the ring, the pendulum was rebalanced by the addition of counterweights, raising the total weight of the pendulum to 191.9 lb. The depth chosen for the ring was based on simple calculations of the maximum expected deflection by bending of an edge-supported plate due to uniform loading over a concentric circular area equal to the projected area of the projectile head [3]. These approximate calculations indicated that the back edge of the least stiff target could be expected to deflect a little more than 1.0 inch with a maximum anticipated load of 10,000 lb, assuming no crush of the honeycomb core.

No changes were made to the air gun except to replace

the pressure gage with one that would allow the use of higher pressures, up to 200 psi. The projectile remained unchanged except that the location of the black/white border on the projectile was moved back an additional 0.5 inch from the front of the projectile to enable the Optfollow camera to track the border for crushes greater than the previously allowed maximum of 1.0 inch The distance that the projectile would be within the FOV of the Optfollow camera was enlarged to about 2.6 inches by moving the stationary black and white borders which define the edges of the usable FOV. This was done to facilitate tracking of the projectile over a longer distance for an anticipated deeper crush. No changes were made to the lasers, the accelerometer, the deflection measurement gage, or to the Nicolet oscilloscope.

Targets

The edge-supported tests required targets much larger than those used in the back-supported tests. The size of the circular targets was selected to be 11.0 inches in diameter. This allows the target to extend about 1/2 inch beyond the edge-support around its circumference. Centrally mounted targets were held in place, prior to being impacted by the projectile, by the use of small amounts of masking tape which connected the top and bottom edges of the specimen directly to the pendulum and held the target flush against the edge-support ring. The ring with the target on it was located so that the projectile would impact it at its center. A total of 10 specimens were tested. Four different

face plate materials were used: 5052 H32 aluminum, with thicknesses t=0.032 inch and t=0.050 inch; polycarbonate (Lexan), t=0.0385 inch; and fiberglass, t=0.030 inch. Also, four different aluminum honeycomb cores were used: 1/4-.001, 1/8-.001, 1/8-.002, and F40-.0019. (Honeycomb core designations are defined as: cell width in inches--wall thickness in inches. F40 designates a non-hexagonal cell shape that allows the core to be formed into doubly curved surfaces.)

Dynamic Test Results

Ten targets were tested; of these, seven were "successful" runs in that they resulted in full data acquisition for the crush. For two tests, the Nicolet did not record the data due to problems with the lasers triggering prematurely or not at all. For a third test, the crush was so severe that the projectile moved outside the FOV of the Optfollow during crush and incomplete data was obtained. Data on these 10 tests is contained in Table 1.

The composition of each target is defined in the first three columns of Table 1. The first column defines the core in terms of cell size in inches (F40 refers to a non-hexagonal "flexcore" cell), and the thickness of the cell walls. The second and third columns show the material and thickness of the face plates.

For each test, the velocity of the projectile just prior to impact was measured by two different methods: using

the measured time for the interruption of the two parallel laser beams spaced 10.33 inches apart, and differentiating the displacement data from the Optfollow system. Although the two velocity measurement systems agreed closely (within 3% on every test), the impact velocity based on the lasers is shown in Table 1 since the lasers are considered more accurate. However, for rebound velocity, the Optfollow data is used because the projectile did not rebound directly through the parallel laser beams after impact. Impact velocities for runs 5 and 10 are approximate because the oscilloscope did not record data for these runs. The impact velocity for these runs is estimated based on the known pressure in the air gun and a graph of air pressure versus projectile velocity.

The deflections of the top and bottom face plates are based on actual measurements of the targets after the test. These measurements are taken after any elastic rebound has taken place, and thus may not show the maximum displacement which occurs during the test. (The issue of elastic rebound of the specimens is covered in the section "Discussion of Test Results".) Core crush percent is obtained by dividing the measured change in core thickness (at the center of the crushed area) by the original core thickness and then multiplying by 100.

The energy absorbed in each run is calculated as $T = 0.5M(V_i^2-V_r^2)-P$, where M is the mass of the projectile and V_i and V_r are its initial and final velocities,

respectively, and P is the kinetic energy of the pendulum (which is very small compared to T). The maximum pressure is based on the maximum force, F = ma, (where m is the mass of the pendulum and a is the acceleration from the accelerometer) divided by the projected area of the projectile head.

The cushion factor, C, is a measure of the efficiency of an energy absorption system. C is defined as the ratio of the peak transmitted stress to the energy absorption per unit volume of the cushion. For the purposes of this calculation, the volume of the cushion is taken as the projected area of the projectile head times the thickness of the honeycomb core. (The thickness of the face plates is not included since they are essentially incompressible.)

Although the cushion factor is not designed to be used for cases in which the "cushion" can bend in addition to crush, it provides a good measure of the relative energy absorption effectiveness of different edge-supported sandwiches. The cushion factors cited here are given solely for the purpose of comparing these edge-supported experiments to each other and are not intended for other uses. Comparison of these cushion factors to those for materials which do not bend may be misleading.

Figures 2 through 8 show crush pressure versus displacement for each of the 7 runs reported in Table 1 for which complete data was obtained. Crush pressure is defined as the load applied divided by the projected area of the

projectile head (6.51 in^2). Displacement refers to the distance that the top face plate moves during impact. Displacement rather than per cent crush is shown on the horizontal axis because the total displacement includes both bending and crushing components. As is seen in Table 1, crushing of the core may account for a very small portion of the total displacement. These plots of crush pressure versus displacement make use of the Optfollow data for displacement measurements and the accelerometer data for acceleration and pressure measurements. The Optfollow record of voltage versus time is converted to displacement versus time based on a static calibration which is performed just prior to the dynamic test. The static calibration is performed by using an x-y table to dial the projectile along the flight path into the FOV in known distance increments. By noting the voltage output by the Optfollow at each increment, a record of voltage versus position is obtained and then used to convert the voltage at any time during impact to position, thus giving a record of displacement versus time. The accelerometer record of voltage versus time is converted to acceleration versus time by multiplying by an experimentally determined calibration factor. The relation F = ma is used to convert accelerations, a, to forces, F, using the mass of the pendulum, m. Force is converted to pressure by dividing by the projected area of the projectile, giving a record of pressure versus time. A computer program is used to join these two records of displacement and pressure versus time

together to give a single record of pressure versus displacement. The details of this data reduction are found in [1].

Figures 9 through 11 show crush pressure vs. displacement for pairs of similar runs in order to facilitate visual comparison of the two runs at the same scale. In each of these figures, both runs have very similar velocities, and have either the same core or the same faces. Figure 9 compares runs 1 and 9, which both have initial velocities of about 835 inches per second and 1/8-.001 cores, but have 0.050 inch and 0.032 inch 5052 aluminum face plates, respectively. Figure 10 compares runs 8 and 7, which both have initial velocities near 940 inches per second and 0.032 inch 5052 aluminum face plates, but have 1/8-.001 and 1/4-.001 cores, respectively. Figure 11 compares runs 2 and 4, which both have initial velocities of about 1210 inches per second and 0.032 inch 5052 aluminum face plates, but have 1/8-.002 and 1/4-.001 cores, respectively.

Quasi-Static Test Results

A single quasi-static test was run. The specimen was made with a 1/8-.001 core and 0.032 inch 5052 aluminum face plates. This test was designed to provide post-rebound face plate deflections as close as possible to those of dynamic test 8 where the target was composed of the same materials. The downward displacement of the projectile was halted and reversed when the maximum deflection reached 0.67 inch with the expectation that the elastic rebound of the specimen

would be a little less than 0.1 inch. In fact, the elastic rebound was 0.11 inch. The final top face plate displacement was 0.56 inch, and the bottom face plate displacement was 0.48 inch, both values being 0.03 inch less than the values for dynamic run 8. The strain rate of the test was about 0.008 in/in/sec. Per cent core crush was 10.4%. The energy absorbed by the specimen was 1738 in-lb, and the maximum pressure was 660 psi. The cushion factor, C, for this test was 1.9. A plot of crush pressure versus displacement for this test is found in Figure 12.

Discussion of Test Results

As can be seen in Table 1, for almost all of the specimens tested dynamically, very little core crush occurred. Most energy absorption seemed to be due to plate bending as the sandwich plate deformed globally under the pressure of the projectile at its center. The two exceptions to this rule are Runs 3 and 4. In Run 3 (see Figure 13), both the top and bottom face plates of 0.0385 inch polycarbonate sheared and cracked during impact. Of the 10 dynamic tests and one static test, this is the only run for which any shearing or cracking of either face plate occurred. In Run 3, local deformation modes predominated over global deformation modes. The sandwich plate did not bend. Rather, the projectile punched right through the sandwich, shearing the plates and the core. A small portion of the specimen, somewhat larger than the projected area of

the head of the projectile was pushed through the specimen and crushed against the pendulum, as if in a back-supported test. The core in this small piece of sandwich was crushed beyond densification, while the rest of the core was almost unaffected. This combination of face plates and core is clearly not optimal for energy absorption with edge-support.

Run 4 is a case in which significant core crush occurred as well as significant bending of the sandwich plate as a whole. As can be seen in the view shown in Figure 14, significant core crush occurred throughout the specimen, not just under the region of contact with the projectile. The top face plate showed significant creasing, with core crush beneath the creases. Also, the specimen underwent considerable plate bending, ending up in an almost conical shape. By utilizing these three different deformation modes, the specimen absorbed a large amount of energy while keeping the maximum pressure low. This run has the best cushion factor of all the dynamic runs for which full data is available. In this case, the combination of core and face plates proved nearly optimal for the amount of energy to be absorbed. The reason that this run showed such an effective energy absorption pattern is that it was the sandwich configuration with the least dense core with face plates that could survive large deformations without failure.

Runs 7 and 9, which have the same sandwich configuration as Run 4, are similar to Run 4 in that a fair amount of core crush as well as some face plate wrinkling

occurred, along with bending of the plate as a whole. These two runs also showed good cushion factors, although not as good as for Run 4.

The specimens for Runs 1, 2, 5, 6, 8 and 10 all looked much like Figure 15. These runs are characterized by very little core crush, little or no creasing of the face plates, local deformation of the top face plate around the edge of the region impacted by the projectile, and bending of the sandwich plate as a whole. Thus, based on observation of the deformation modes involved in each run, sandwiches made of 1/4-.001 cores and 0.032 inch 5052 aluminum face plates seem to be the most effective in their energy absorption of the samples tested.

The dynamic crush versus displacement plots, Figures 2 through 8, demonstrate a fairly constant pattern during impact. The projectile contacts the specimen and the crush pressure rises to some maximum value as the displacement increases. As the crush pressure starts to drop, the displacement continues to increase until it reaches its maximum value. Then, as the crush pressure drops to zero, the displacement begins to decrease. Once the pressure drops to zero, the projectile leaves contact with the specimen and flies off at its rebound velocity. The oscillations of the pressure about zero after the projectile leaves contact with the specimen are due to vibration in the pendulum. Just as an increase of displacement indicates that the specimen is being displaced by the projectile, so a decrease in

displacement, while the projectile is in contact with the specimen, indicates that the specimen is returning to its original position. The dynamic crush pressure versus displacement plots seem to indicate that the specimen typically rebounds elastically about 0.1 inch as the crush pressure drops to zero. This elastic rebound of the specimen is seen most clearly in the quasi-static plot of crush pressure versus displacement in Figure 12. As the pressure on the specimen drops from its maximum value to zero, the specimen rebounds elastically about 0.1 inch. This elastic rebound effect was clearly visible during the quasi-static test.

As can be seen in Figure 9, where test results for the same core (1/8-.001) with two different face plates (0.050 inch and 0.032 inch 5052 Al.) are compared, the thinner plate is a much better choice for absorbing energy. The maximum pressure is much less and the cushion factor is thus much better for the run with the thinner skin. Although the core crushed about the same amount in both Runs 1 and 8, the sandwich as a whole bent much more in Run 8, showing that the thinner plate is a better choice at this energy level. The thinner plate allows the sandwich plate to bend more easily while still being strong enough to distribute the impact energy over a large area and not shear through. However, the thinner plate would be the better choice only for impacts which do not exceed the energy absorbing capacity of the sandwich. By examining the specimen from Run

8 carefully and comparing it to other specimens, it appears that only a fraction of its energy absorbing capacity has been consumed. It would appear to be able to handle about five times the energy it absorbed in Run 8. For impact energy levels much higher than those seen in Runs 1 and 8, it is possible that a thicker face plate would be advantageous. Thus, the amount of energy to be absorbed plays a significant role in the selection of the best face plates. The 0.050 inch 5052 aluminum plates were just too thick for optimal absorption of the amount of energy present in Run 1.

From Figure 10, in which runs with different cores (1/4-.001 and 1/8-.001) and the same face plates (0.032 inch 5052 aluminum) are compared, it is seen that the specimen with the less dense core, Run 7, is more efficient for energy absorption. The maximum crush pressure is much less for Run 7. The same observation can be made from Figure 11, in which runs with two different cores (1/4-.001 and 1/8-.002) and the same face plates are compared: the less dense core is a better choice for minimizing transmitted load while maximizing energy absorbed.

Thus, of the four sandwich configurations compared in Figures 9, 10 and 11, a 1/4-.001 core with 0.032 inch 5052 aluminum plates would be expected to be the most efficient in terms of energy absorption. This conclusion agrees with that drawn from an examination of the deformation modes involved in each test. However, if the energy to be absorbed

is very large, it is possible that a denser core or thicker face plates, or both would be preferred. For example, Run 6 demonstrates that as the energy absorbed becomes higher, the cushion factor for a sandwich with a denser core improves. A close examination of the specimen from Run 4, with a 1/4-.001 core and 0.032 inch 5052 aluminum face plates indicates that probably more than half of its energy absorption capability has been consumed. The core has been crushed to less than half of its original thickness, and the back plate has displaced almost 1 inch. As a rough estimate, it would seem that the energy absorption capacity of this sandwich configuration is about 5000 to 6000 in-lb. For protection from impacts involving more energy than this, a denser core or thicker face plates should be used.

An interesting feature common to most of the plots of dynamic crush pressure versus displacement is a sort of loop in the curve near maximum displacement, where the pressure goes down, then up and then down again in a very short distance as the projectile is about to separate from the specimen. This phenomenon was not present in the back-supported sandwich tests of [2]. This phenomenon is also clearly not present in the quasi-static test shown in Figure 12. Another odd feature common to each of the tests is the fact that no crush pressure is sensed by the accelerometer until after the specimen has been crushed about 0.1 inch. Because it was suggested that this phenomenon may be due to the test set up or to the data reduction techniques used, an

alternative method for obtaining crush pressure versus displacement was employed. In this alternative method the accelerometer data is not used at all. Instead, the Optfollow displacement versus time data is differentiated twice to obtain acceleration versus time data. This differentiated data has a high level of noise in it, and a data smoothing program is used to reduce the noise. The acceleration data is then converted to force data using the relation F = ma, where F is the force, m is the mass of the projectile, and a is the Optfollow acceleration. The force data is then converted to crush pressure by dividing it by the projected area of the projectile. The resulting pressure versus time data is then combined with the Optfollow displacement versus time data to give a plot of crush pressure versus displacement which is based entirely on the Optfollow data.

Three of the tests, Runs 2, 7 and 8, have been re-analyzed using the doubly differentiated Optfollow displacement data to provide information on pressure. Plots of crush pressure versus displacement for these three runs are shown in Figures 16 through 18. Although the Optfollow data was considered less reliable than the accelerometer data for determining crush pressure for back-supported tests, the reverse seems true for edge-supported tests. The plots in Figures 16 through 18 lack the odd loop which appears in Figures 1 through 7. Additionally, the Optfollow pressure versus displacement plots are much more

believable than the plots based on accelerometer data, since they show crush pressure beginning right at impact - not only after the sandwich has deen crushed about 0.1 inch.

For the back-supported dynamic sandwich tests reported in [2], no large difference was noticed between the doubly differentiated Optfollow data and the accelerometer data. A close examination of the tset set up provides the reason for why the accelerometer data may be much less reliable for the edge-supported tests than it was for the back-supported tests. During impact of a back-supported specimen, the load path from the region of contact between the projectile and the target to the accelerometer was very short and very direct. The impact loads traveled about 3.5 inches through the solid steel pendulum to get from the region of contact to the accelerometer. Thus, the accelerometer recorded accelerations very similar to those experienced by the specimen.

However, during impact of an edge-supported specimen, the load path from the region of contact to the accelerometer is both long and complex. From the contact region the impact load must travel 5 inches radially through the target to the edge support ring. Then, the load must travel 1.5 inches along the 0.15 inch thick wall of the ring to reach the pendulum, and then must travel over 6 inches diagonally through the steel pendulum to reach the accelerometer. Thus, the total path from the contact region to the accelerometer is more than 12 inches. This long

complex load path accounts for the "delay" seen in each of Figures 2 through 11, in which the accelerometer senses no acceleration until about 0.1 millisecond after the specimen has been impacted. Thus, it is apparent that the accelerometer is too far removed from the region of impact to accurately present the forces at that location. Placement of the accelerometer directly on the back side of the specimen would eliminate this problem, but this would require major changes to the test set up.

The Optfollow, on the other hand, is not expected to be significantly less reliable for edge-supported tests than it was for back-supported tests. For edge-supported tests, the projectile border, which is being tracked by the Optfollow, is only about 0.5 inch farther from the region of impact at the projectile head than it was for back-supported tests. This does not make any significant difference in the quality of data obtained from the Optfollow. The doubly differentiated Optfollow data, which is considered somewhat less reliable than the accelerometer data for back-supported tests, is nevertheless considered to provide a much more reliable record of acceleration at the region of impact for edge-supported tests than does the accelerometer which is mounted on the back of the pendulum.

A comparison of Figures 16 through 18 (which are based solely on Optfollow data) to Figures 3, 8 and 9, respectively (which make use of the accelerometer data) shows three main differences. First, for the plots based on

the doubly differentiated Optfollow data, the crush pressure begins to rise as soon as contact occurs. Second, for these plots, no strange loop occurs near maximum displacement. Third, the maximum pressure from the Optfollow data is about 60 per cent of that given by the accelerometer.

By using the Optfollow acceleration data instead of the accelerometer data, two columns of Table 1 would change. The maximum pressure would be reduced to about 60 per cent of the value shown. Also, the cushion factor, C, which is based on the maximum pressure value, would decrease by the same ratio. All other data in Table 1 would remain unaffected. None of the comparisons between different sandwich materials made on the basis of information from Table 1 or Figures 2 through 11 would be significantly affected since the data from each run would be affected proportionately.

In order to obtain a valid comparison between edge- and back-supported tests, the doubly differentiated Optfollow data is used for the edge-supported tests. Runs 2 and 7 are compared to back supported tests (reported in [2]) of the same sandwich configuration in Figures 19 and 20, respectively. In Figure 19, the back-supported test was run at a projectile velocity of 1339 inches per second, which is 11.4 per cent higher than the velocity in Run 2. The energy absorbed by the back-supported specimen was 4040 in-lb. Ratioing this energy by the square of the impact velocities gives an estimated energy absorbed of 3255 in-lb for a velocity of 1201 inches per second. This is essentially

identical to the energy absorbed by the edge-supported specimen: 3257 in-lb. Hence, no difference is seen in the quantity of energy absorbed for the two test methods. However, there is a big difference in the maximum pressure experienced by the specimens. The back-supported specimen absorbed energy at a maximum crush pressure which is 90 per cent higher than that for the edge-supported test. Therefore the edge-supported specimen is a much more efficient energy absorber.

In Figure 20, The back-supported test was run at a velocity of 762 inches per second, which is 14.5 per cent less than the velocity in Run 7. The energy absorbed by the back-supported specimen was 1370 in-lb. Ratioing this energy by the square of the velocities gives an estimated energy absorbed of 1873 in-lb for a velocity of 891 inches per second. This is not significantly different from the energy absorbed in Run 7: 1829 in-lb. Therefore, no significant difference is observed in the quantity of energy absorbed by the two methods. However, once again, the back-supported test had a much higher maximum crush pressure, showing that the edge-supported specimen is a much more efficient energy absorber.

The final plot, Figure 21, shows a comparison of quasi-static and dynamic crushes of the same edge-supported sandwich configuration: 1/8-.001 core and 0.032 inch 5052 aluminum faces. The dynamic test data is that from Run 8 using the doubly differentiated Optfollow data for pressure.

The plot shows graphically that there is no significant difference between the pressure versus displacement curves for the two tests. Both specimens absorb about the same amount of energy at about the same crush pressure. The only significant difference between the two plots is that the quasi-static test was stopped too early, before it had reached the same displacement as the dynamic test.

Conclusions

The primary difference between back-supported and edge-supported dynamic crush tests of honeycomb sandwiches is the addition of a plate bending deformation mode for edge-supported tests. An examination of the results of 10 dynamic edge-supported tests shows that the most effective energy absorbing system is one that combines several different energy absorption deformation modes. Of the specimens tested, those with 1/4-.001 cores and 0.032 inch 5052 aluminum face plates were judged most efficient in their energy absorption capabilities because they exhibited significant energy absorption through core crush as well as by plate bending and face creasing. However, the selection of the best sandwich configuration for a given situation must also take into consideration the amount of energy to be absorbed, constraints on weight or volume, maximum allowable deflections and the ratio of contact area to sandwich plate size.

A comparison of edge-supported tests to back-supported

tests shows clearly that the edge-supported specimens are much more effective at energy absorption. For impacts involving the same amount of energy, edge-supported tests showed a much lower maximum crush pressure than back-supported tests. The reason for this improvement seems to be that the edge-supported tests included the additional energy absorption deformation mode of bending of the sandwich as a whole. Thus, the edge-supportes sandwich provides better protection from impact.

References

1. G. H. Smyers, Energy Absorption of Aluminum Honeycomb, (Master's Thesis) Mechanical Engineering Department, University of California at Berkeley, June, 1990.

2. W. J. Beckmann, Energy Absorption Characteristics of Honeycomb Sandwich Plates, (Master's Thesis) Mechanical Engineering Department, University of California at Berkeley, Fall, 1990.

3. R. J. Roark, Formulas for Stress and Strain, 4th ed., McGraw-Hill, Inc., 1965, p216.

TABLE 1
DYNAMIC TEST RESULTS ON EDGE-SUPPORTED SANDWICH SPECIMENS
Original Core Thickness of the 5052 Al. Honeycomb: .75 in

Run No.	Composition Core[1]	Face Plates Material	Face Plates Thickness in	Velocity Impact in/s	Velocity Rebound in/s	Face Plate Deflection top in	Face Plate Deflection bottom in	Core Crush %
1	1/8-.001	5052 Al.	.050	829	-266	.34	.26	10.2
2	1/8-.002	5052 Al.	.032	1201	-281	.55	.54	0.8
3	F40-.0019	Lexan	.0385	1480	-	>2.0	>1.5	84.8
4	1/4-.001	5052 Al.	.032	1219	-178	1.35	.95	52.8
5	F40-.0019	Fiberglass	.030	~800	-	.35	.33	2.7
6	1/8-.002	5052 Al.	.032	1493	-392	.82	.81	1.3
7	1/4-.001	5052 Al.	.032	891	-168	.81	.56	32.6
8	1/8-.001	5052 Al.	.032	987	-268	.59	.51	11.4
9	1/4-.001	5052 Al.	.032	842	-178	.73	.53	26.4
10	1/8-.002	5052 Al.	.050	~2000	-	.83	.77	8.5

Run No.	Pendulum Kinetic Energy in-lb	Energy Absorbed in-lb	Max Pressure psi	Cushion Factor C	Observations[2] Face Plates	Observations[2] Core
1	29	1444	1590	4.9	a	B
2	55	3202	1732	2.7	a	A
3	-	-	-	-	e	C
4	48	3426	813	1.2	d	B
5	26	-	-	-	a	B
6	85	4873	1870	1.9	a	A
7	27	1802	535	1.5	c	B
8	41	2115	1166	2.7	b	B
9	25	1593	664	2.0	c	B
10	-	-	-	-	a	B

[1] Honeycomb core designations are defined as: cell width in inches--wall thickness in inches. (F40 designates a non-hexagonal cell shape that allows the core to be formed into doubly curved surfaces.)

[2] Observations are defined as follows:

a No creases in faces.
b Very minor creases in top face that do not extend to edge.
c Moderate creases in top face that do extend to edge.
d Major creases in both top and bottom faces that do extend to edge.
e No creases in face, but both face plates sheared through.

A Shear bands in core at edges of impacted region only.
B Diagonal shear bands in core throughout specimen, running toward center of specimen from top face to bottom face.

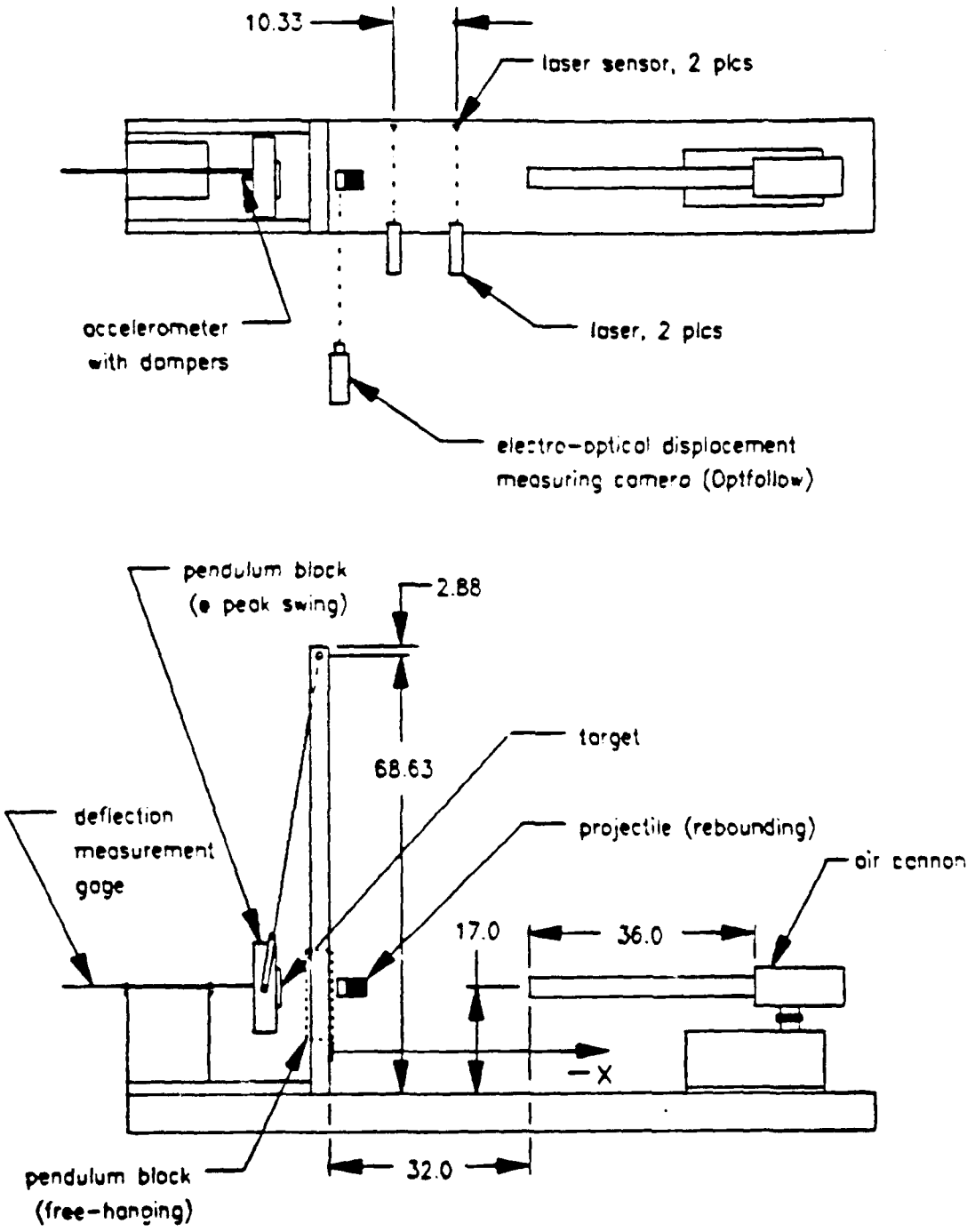

Figure 1. . Equipment Configuration:
Dynamic Crush Test

Note:
Dimensions in inches.

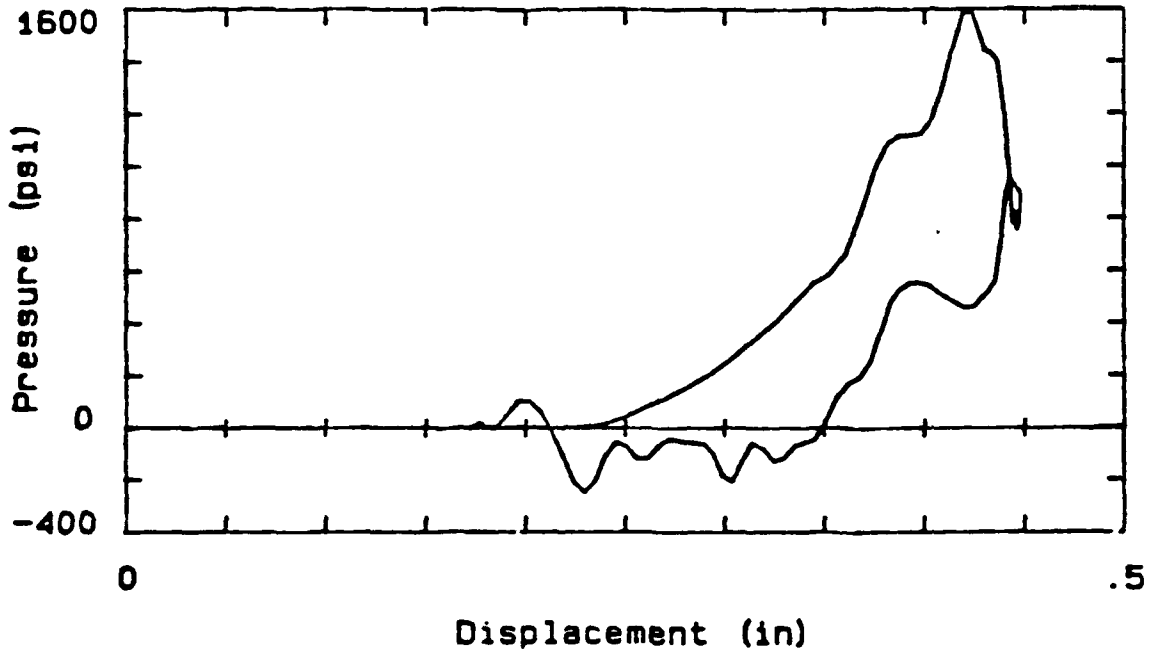

Figure 2. Dynamic Pressure vs. Displacement for Run 1: 1/8-.001 core, .050 in 5052 Al. faces

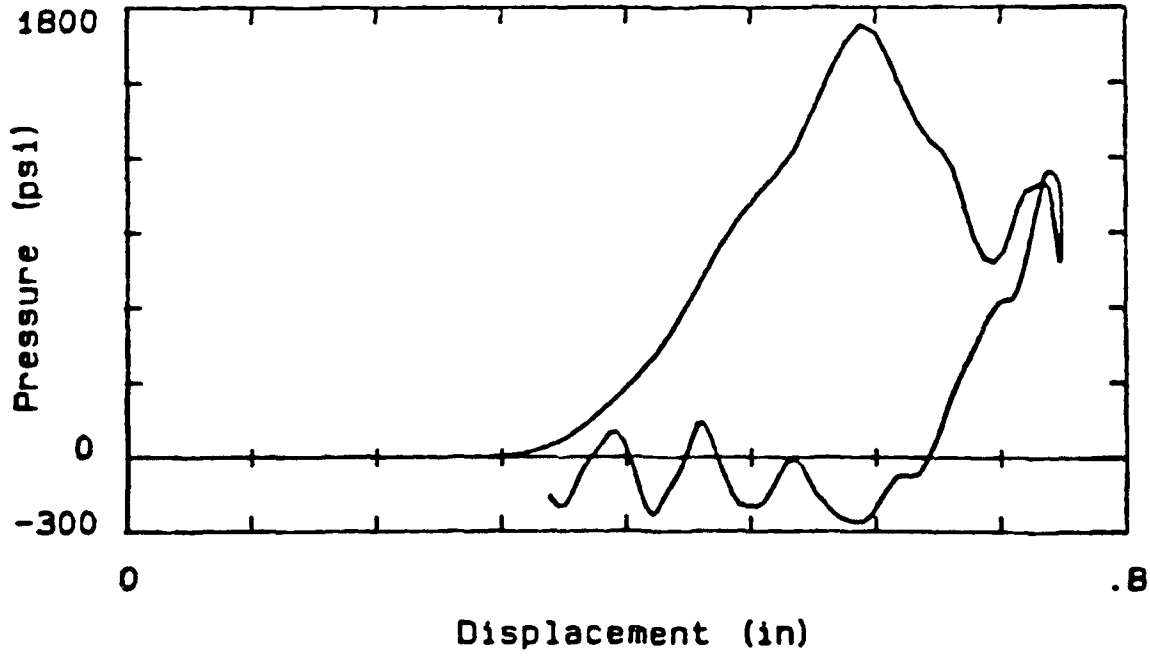

Figure 3. Dynamic Pressure vs. Displacement for Run 2: 1/8-.002 core, .032 in 5052 Al. faces

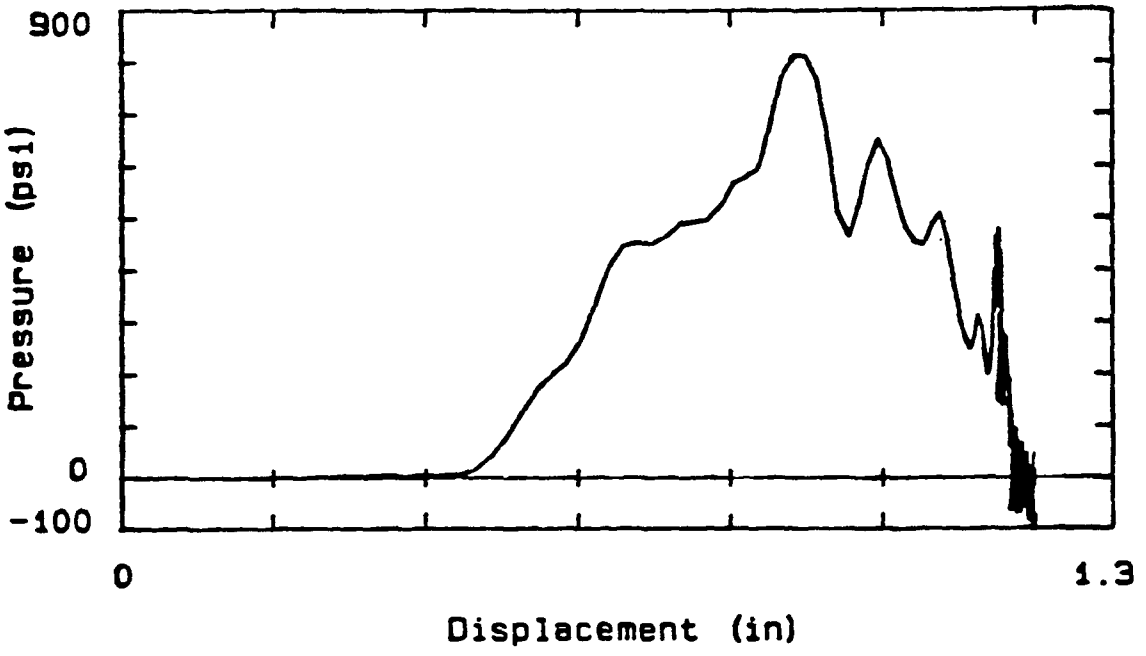

Figure 4. Dynamic Pressure vs. Displacement for Run 4: 1/4-.001 core, .032 in 5052 Al. faces

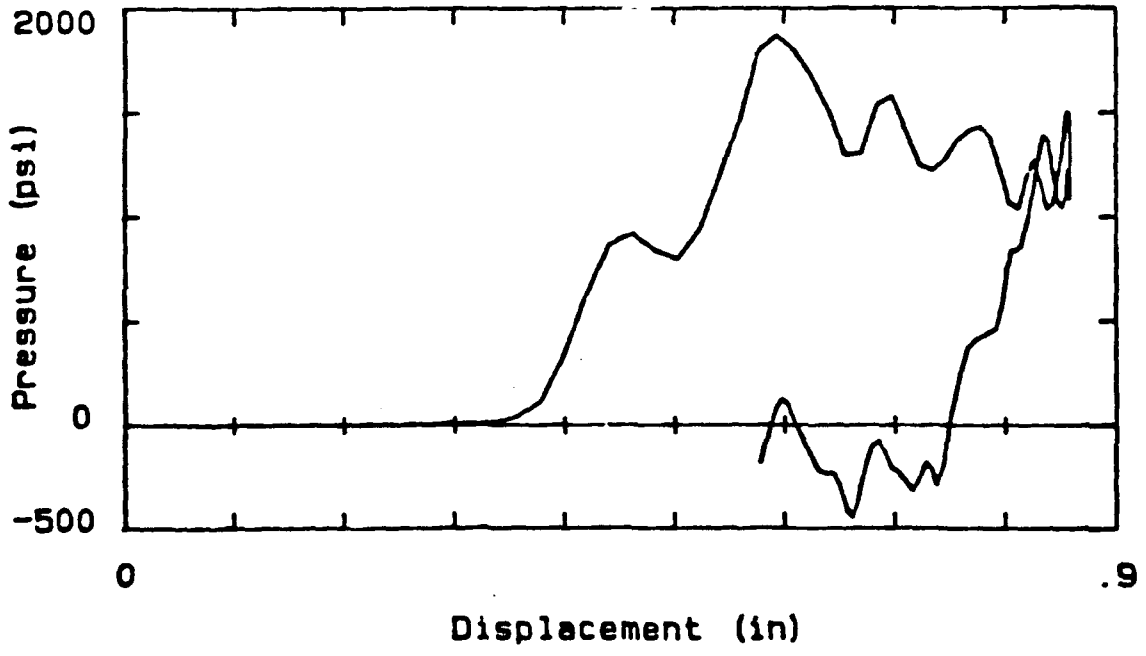

Figure 5. Dynamic Pressure vs. Displacement for Run 6: 1/8-.002 core, .032 in 5052 Al. faces

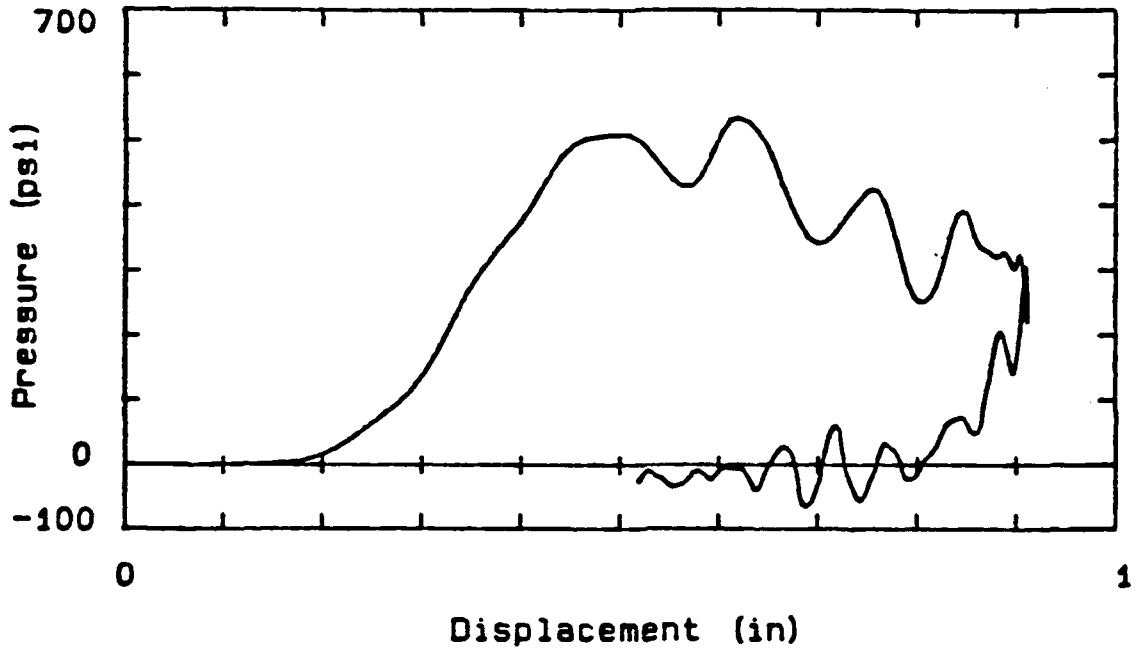

Figure 6. Dynamic Pressure vs. Displacement for Run 7: 1/4-.001 core, .032 in 5052 Al. faces

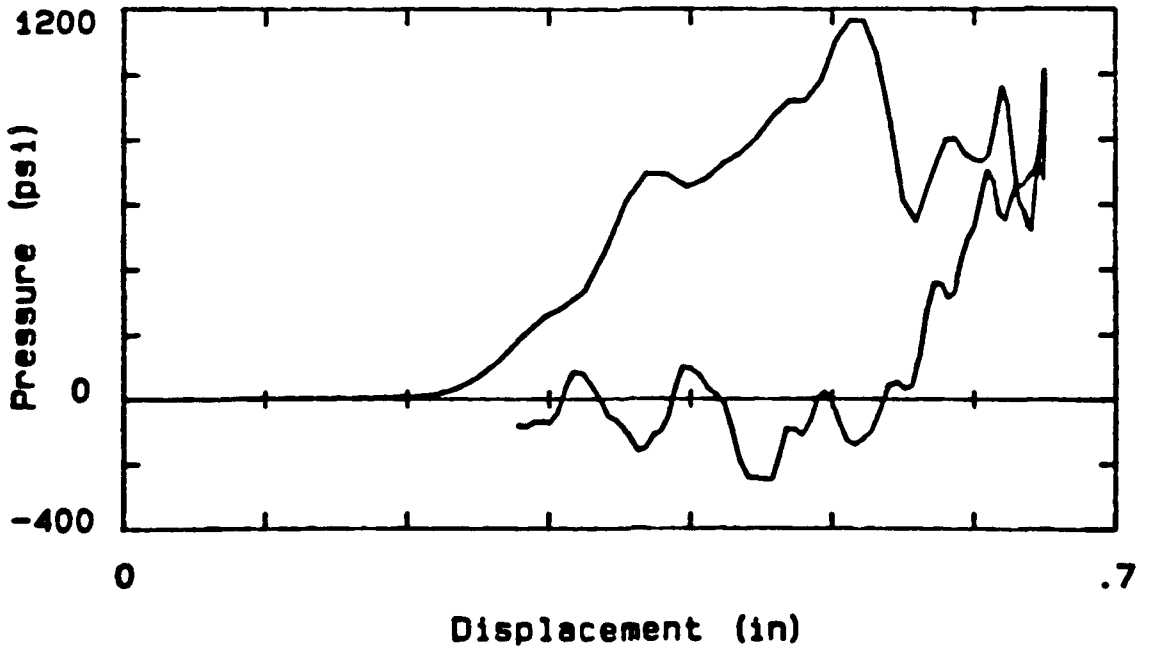

Figure 7. Dynamic Pressure vs. Displacement for Run 8: 1/8-.001 core, .032 in 5052 Al. faces

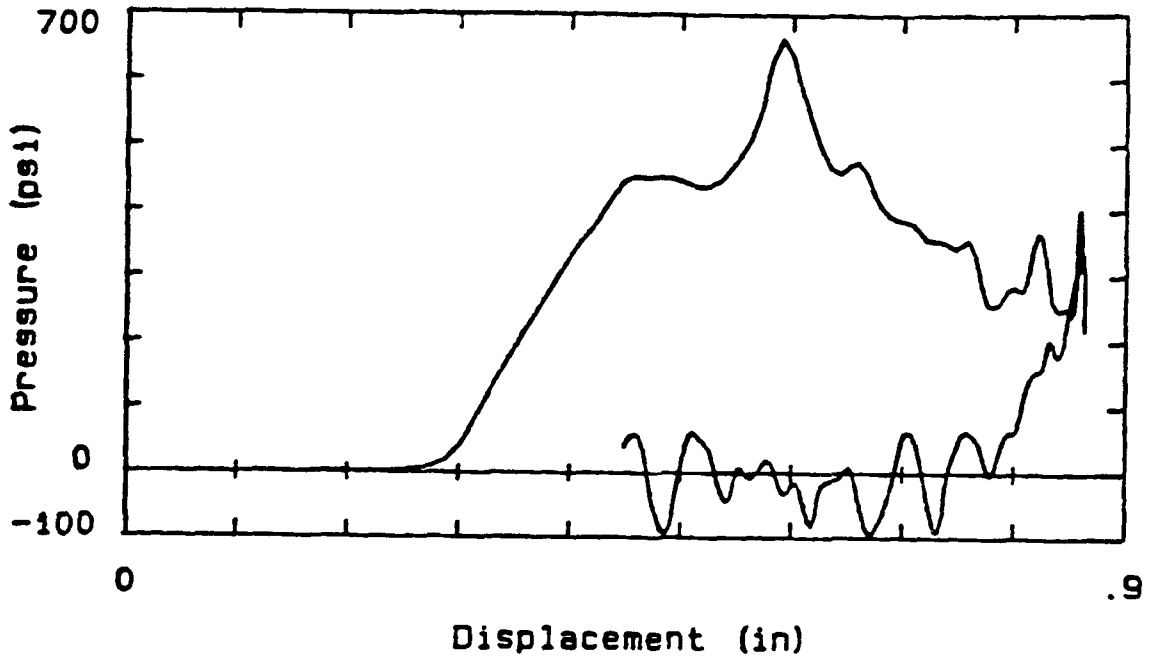

Figure 8. Dynamic Pressure vs. Displacement for Run 9: 1/4-.001 core, .032 in 5052 Al. faces

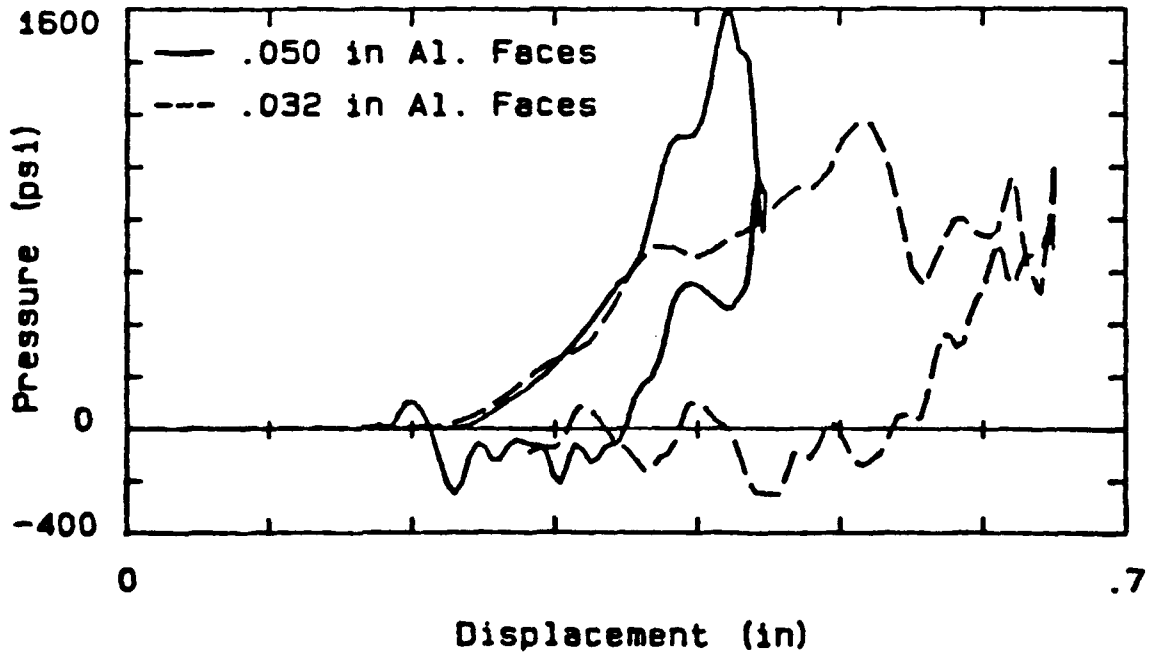

Figure 9. Dynamic Pressure vs. Displacement for Runs 1 & 4
1/8-.001 core, .050 & .032 in 5052 Al. faces

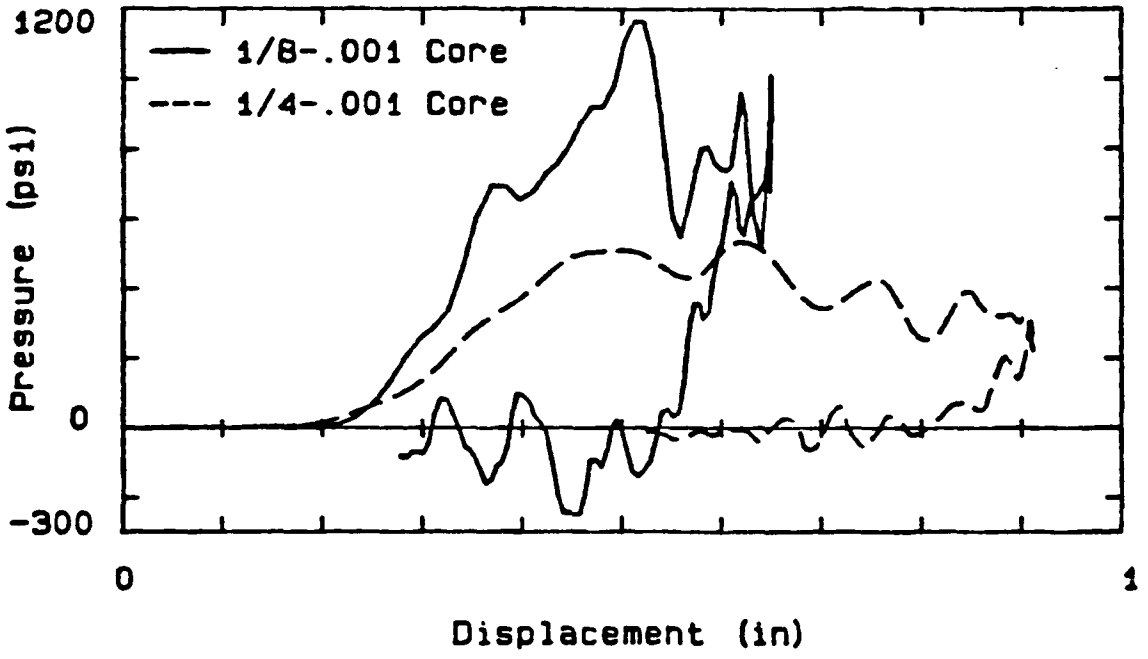

Figure 10. Dynamic Pressure vs. Displacement for Runs 8 & 7
1/8-.001 & 1/4-.001 cores, .032 in 5052 Al. faces

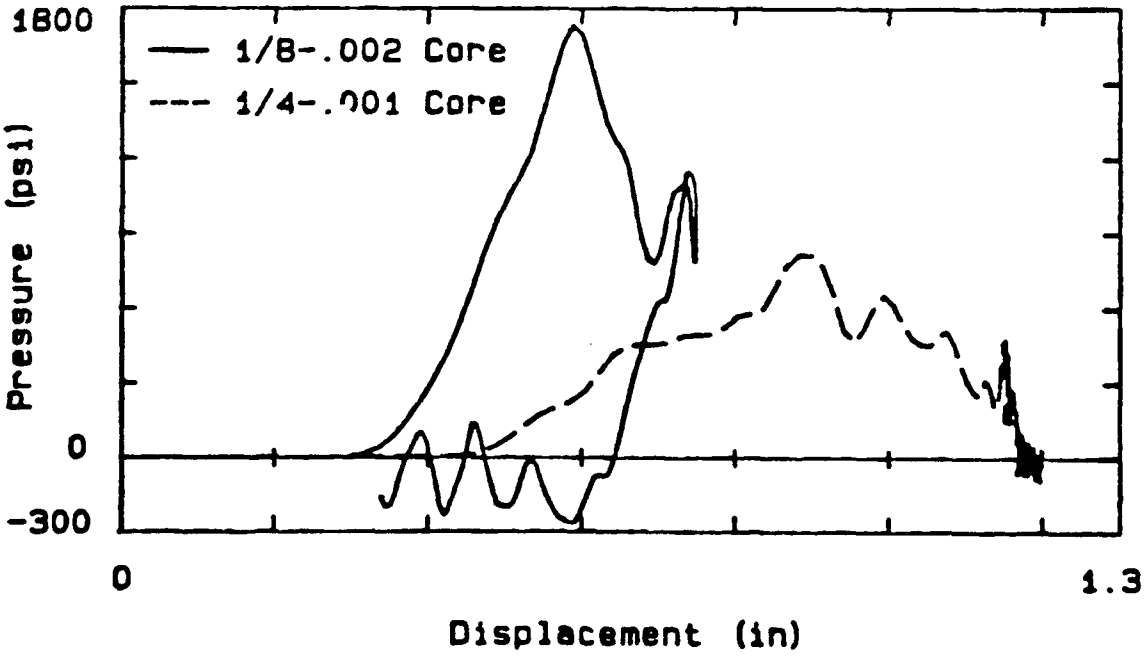

Figure 11. Dynamic Pressure vs. Displacement for Runs 2 & 4
1/8-.002 & 1/4-.001 cores, .032 in 5052 Al. faces

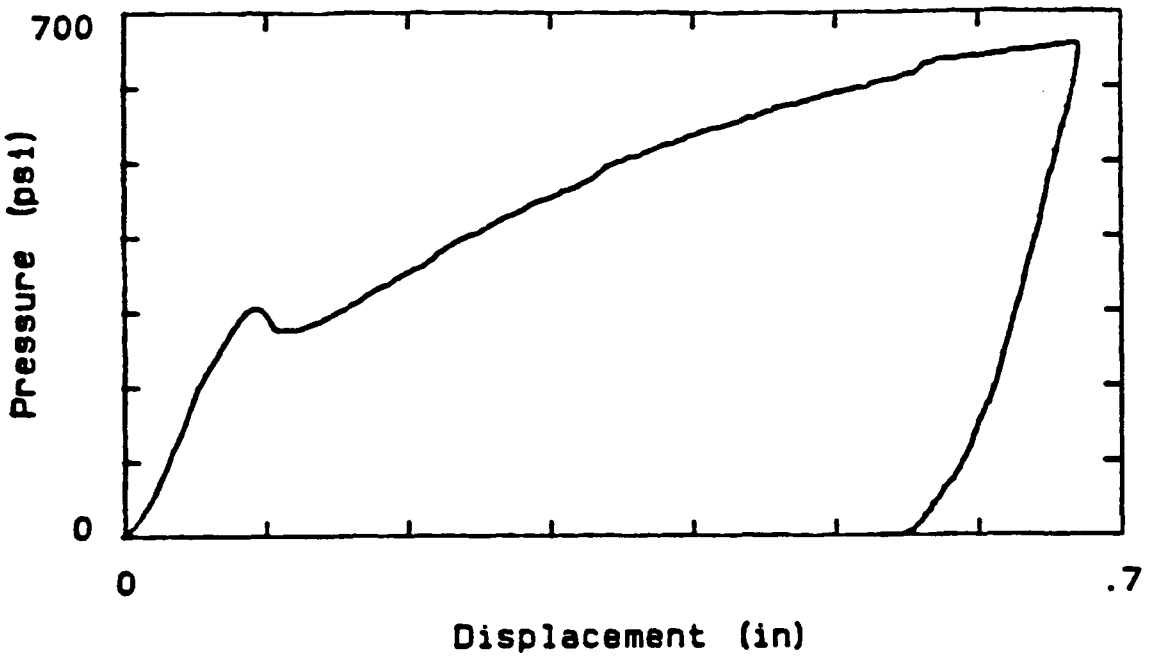

Figure 12. Quasi-static Pressure vs. Displacement
1/8-.001 core, .032 in 5052 Al. faces

Figure 13. Top View of Specimen from Run 3:
F40-.0019 core, .0385 in Polycarbonate faces

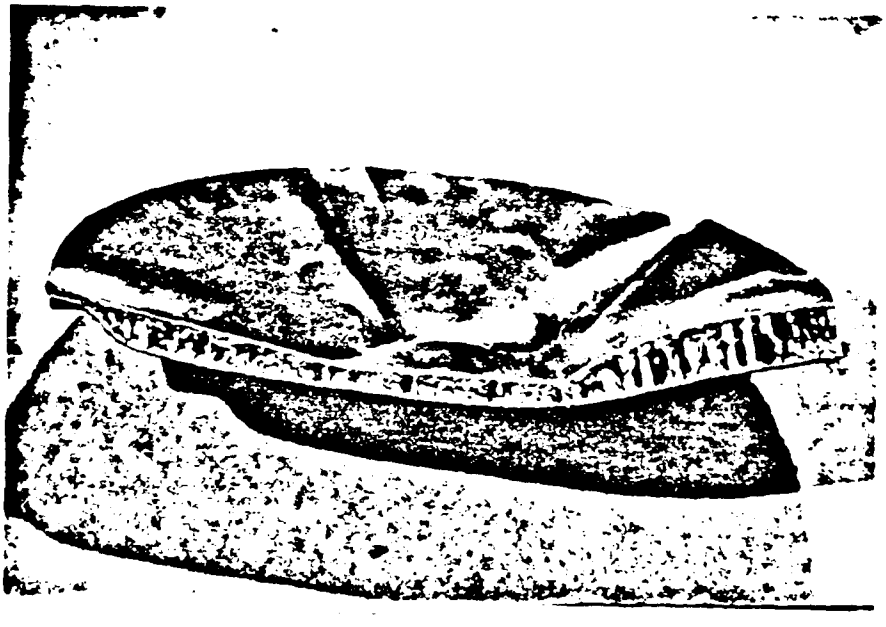

Figure 14. Side View of Half of Specimen from Run 4:
1/4-.001 core, .032 in 5052 Al. faces

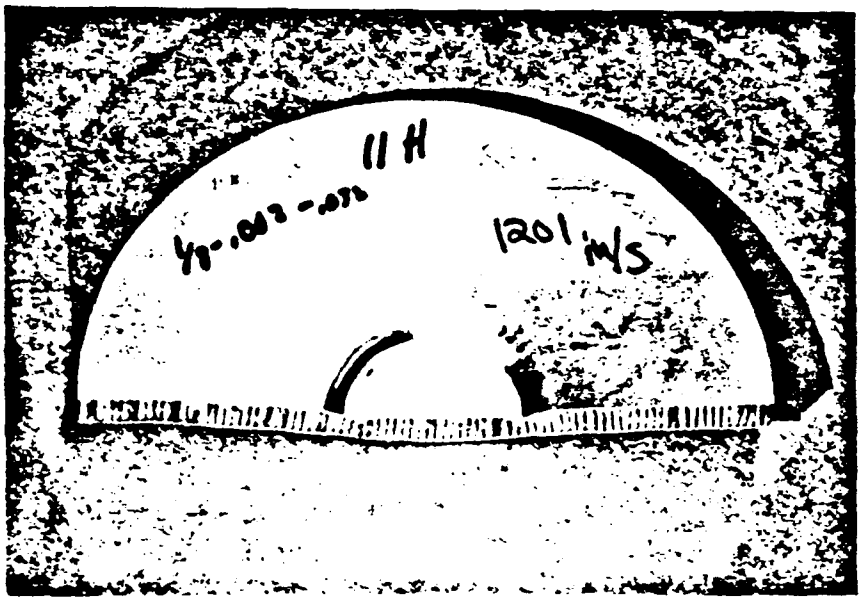

Figure 15. Side View of Half of Specimen from Run 2: 1/8-.002 core, .032 in 5052 Al. faces

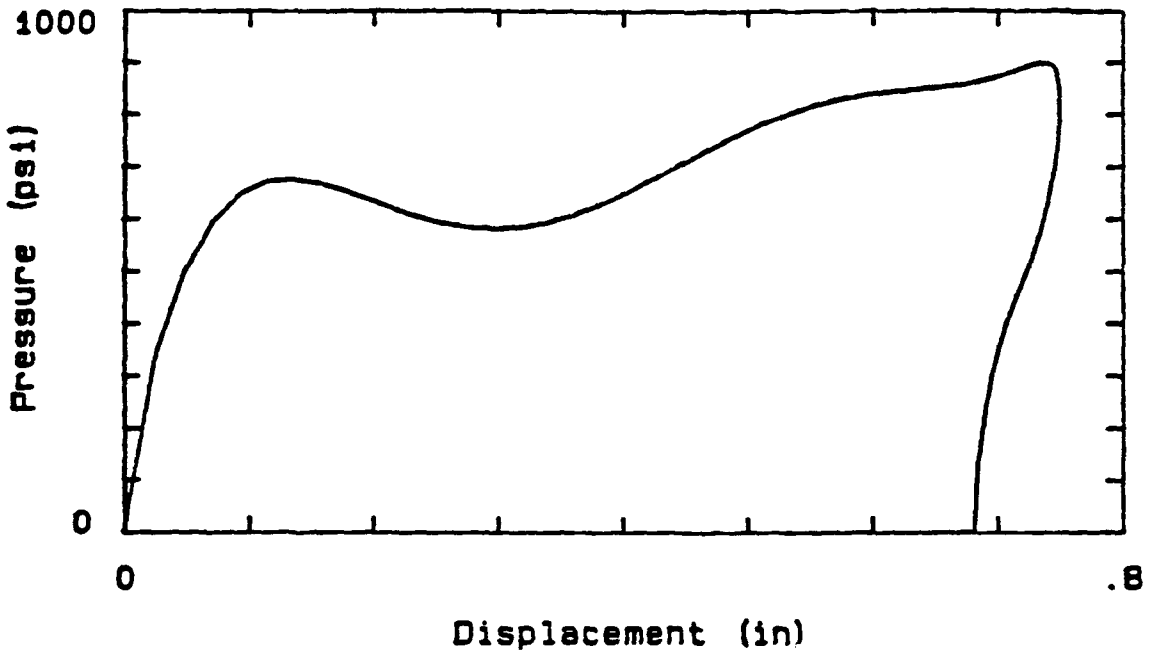

Figure 16. Dynamic Pressure (from Optfollow) vs Displacement for Run 2: 1/8-.002 core, .032 in 5052 Al. faces

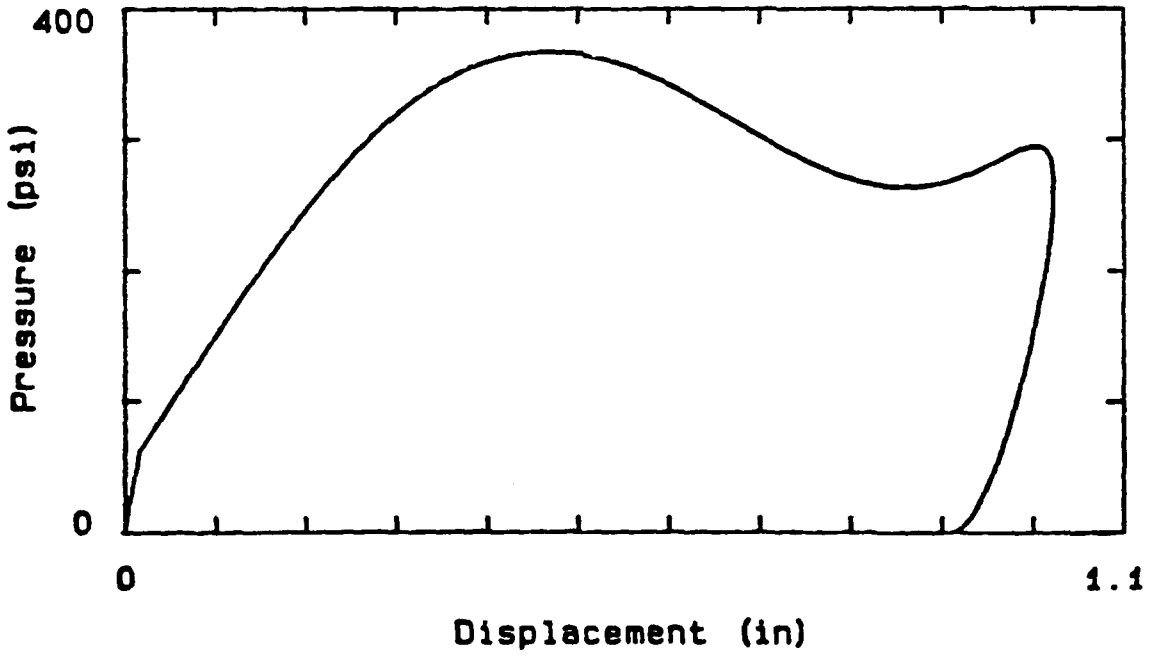

Figure 17. Dynamic Pressure (from Optfollow) vs. Displacement for Run 7: 1/4-.001 core, .032 in 5052 Al. faces

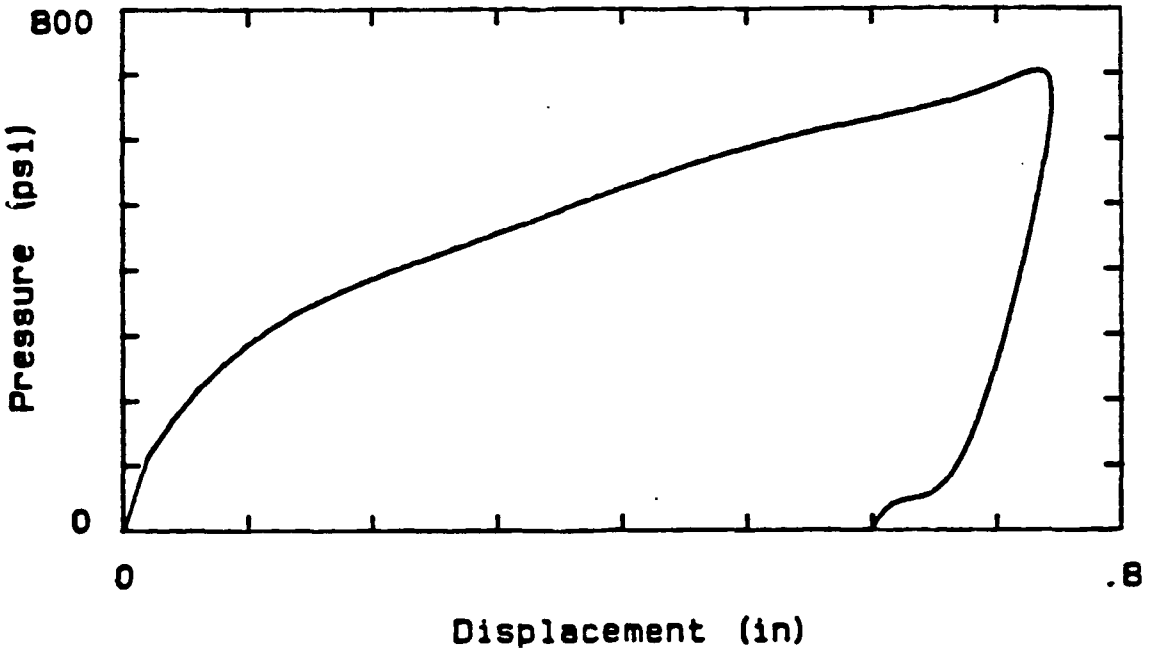

Figure 18. Dynamic Pressure (from Optfollow) vs. Displacement for Run 8: 1/8-.001 core, .032 in 5052 Al. faces

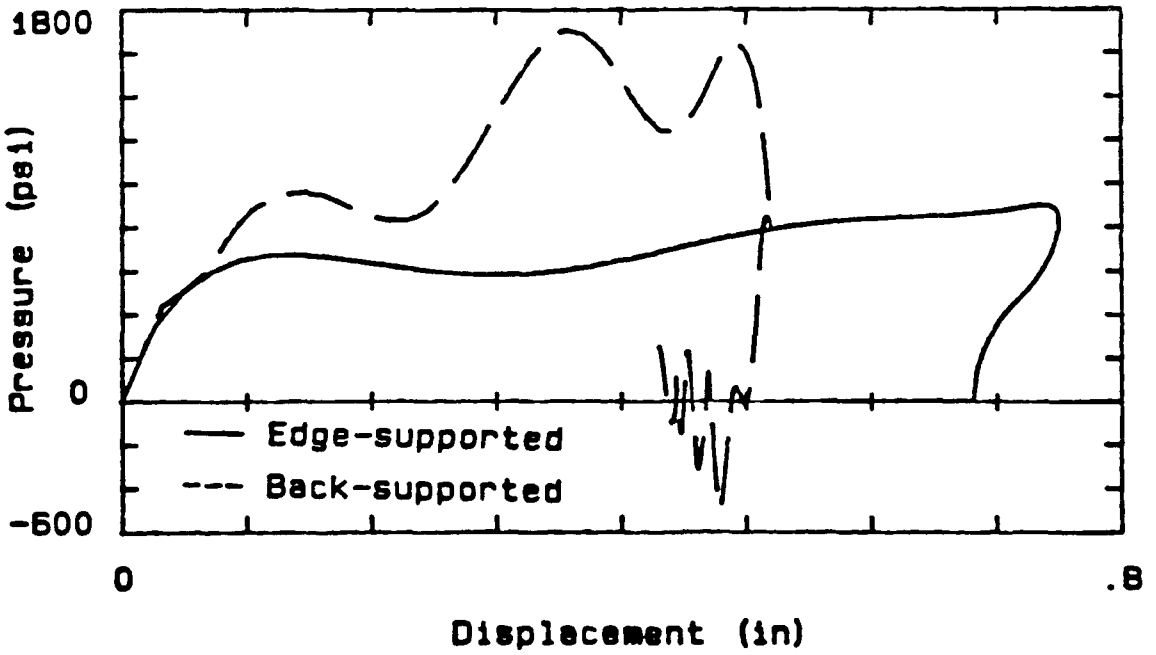

Figure 19. Edge-supported (Run 2, using Optfollow data) and Back-supported Dynamic Pressure vs. Displacement: 1/8-.002 core, .032 in 5052 Al. faces

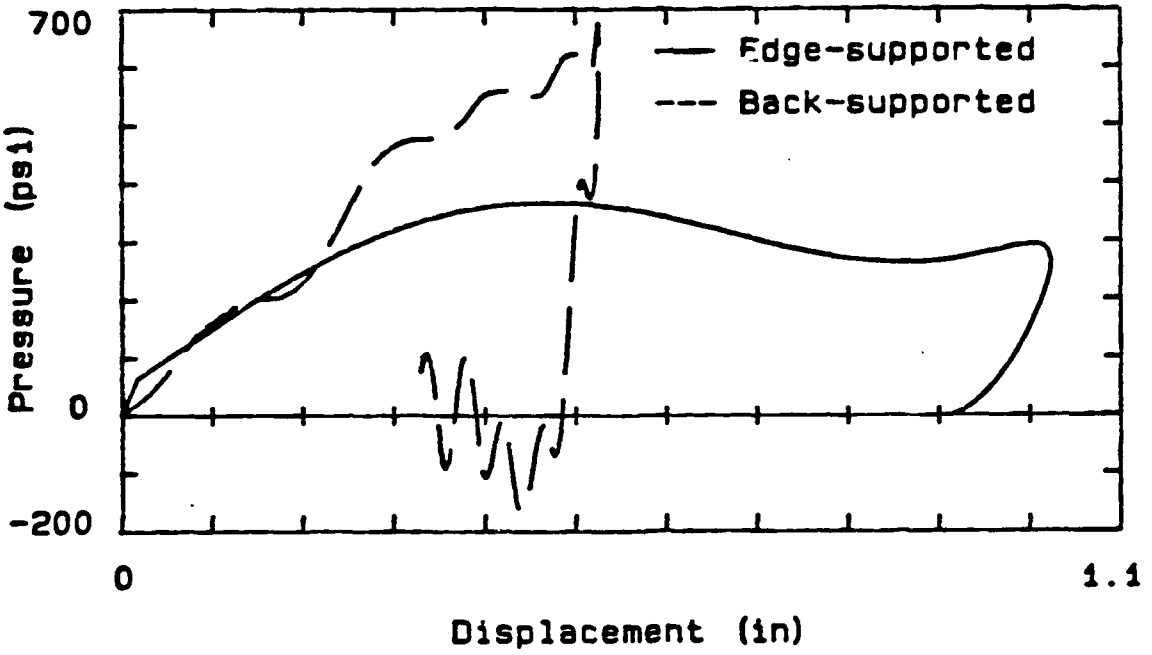

Figure 20. Edge-supported (Run 7, using Optfollow data) and Back-supported Dynamic Pressure vs. Displacement: 1/4-.001 core, .032 in 5052 Al. faces

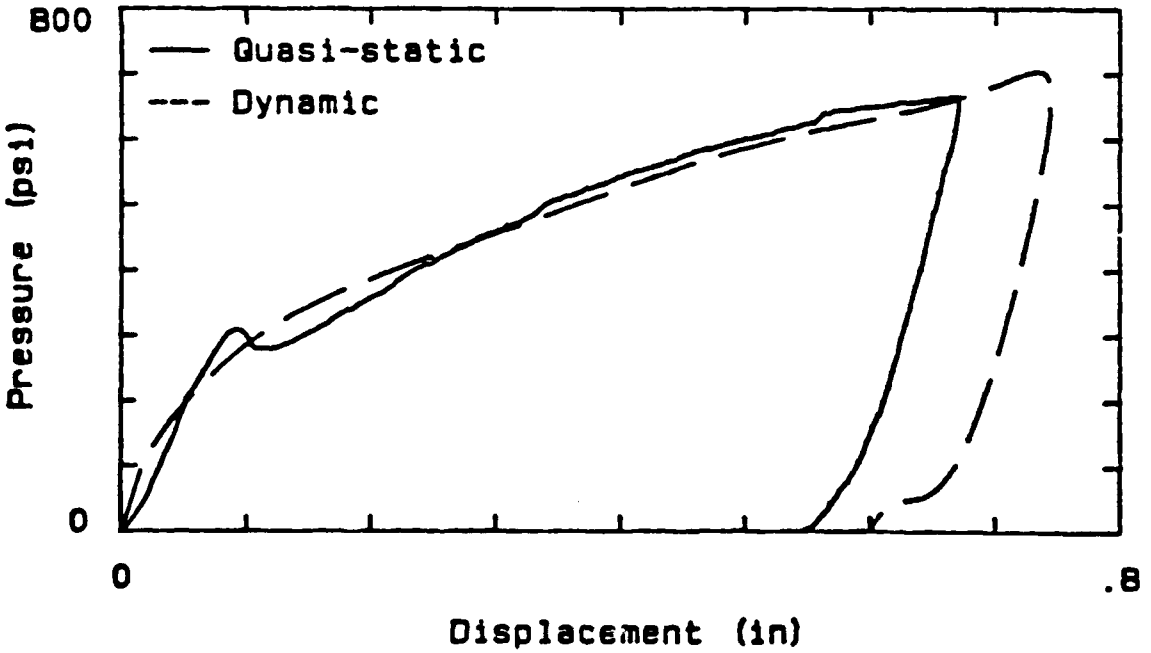

Figure 21. Quasi-static and Dynamic (Run 8, using Optfollow data) Pressure vs. Displacement: 1/8-.001 core, .032 in 5052 Al. faces

APPENDIX C

Influence of the Accumulated Mass of Honeycomb on the Impact of a Rigid Projectile on an Infinite Rigid-Plastic Sandwich Plate

ABSTRACT

The influence of the honeycomb mass accumulating on the front plate of a sandwich system with a honeycomb core impacted by a rigid projectile is presented. The plate is assumed to be rigid perfectly-plastic and to obey the Tresca yield condition and associated flow rule. The honeycomb is modeled as a continuum with varying density. The effect of the additional mass is shown to be negligible.

1. INTRODUCTION

In a previous report (1989), the response of a rigid perfectly-plastic plate to impact by a rigid projectile was discussed. To obtain a simple formulation, the effect of the accumulating mass behind the front plate after impact was neglected as a first approximation.

In this paper, a more general formulation, including mass effect, is presented. The results are compared to the previous ones in order to assess the influence due to the mass of the crushed honeycomb.

2. PRELIMINARY ASSUMPTIONS

The honeycomb foundation is assumed to behave as a continuous media with varying density: a first layer corresponding to the crushed honeycomb in contact with the front plate and a second layer unaltered by the impact of the projectile. The behavior of the honeycomb is taken to be rigid perfectly-plastic in the x_3-direction.

The plate is assumed to be rigid perfectly-plastic. The two-moment limited interaction yield surface proposed by Hodge (1960) is used along with the associated flow rule.

The yield criterion is shown in Figure 2 where M_r and M_θ are, respectively, the radial and circumferential bending moments per unit length and N_r and N_θ are the radial and circumferential membrane forces. M_0 and N_0 are, respectively, the conventional fully-plastic moment and membrane

force for the plate given by:

$$N_0 = \sigma_y \, h \quad , \quad M_0 = \sigma_y \, \frac{h^2}{4} \tag{1}$$

where h is the thickness of the plate and σ_y the yield stress in simple tension.

3. CONSERVATION OF MASS

Before impact, the honeycomb has a uniform density ρ_0 and a thickness h_0. After complete crush, the density is increased to $\hat{\rho}$ and the thickness reduced to $\hat{h}$. The conservation of mass before impact and after complete crush yields a relation between ρ_0 and $\hat{\rho}$:

$$\rho_0 h_0 = \hat{\rho} \hat{h} \tag{2}$$

At a time t after impact, from the kinematics of the plate-honeycomb system, a relation between the initial height h_0 of the honeycomb and the deflection w of the plate can be expressed:

$$w + h_c + h_u = h_0 \tag{3}$$

where h_c and h_u are respectively the thickness of the crushed and the unaffected regions. This is based on the assumption that after impact, the honeycomb crushes in a zone near the plate to a certain thickness while the remaining region is intact.

The conservation of mass for times t_0 and t yields:

$$h_c \, \hat{\rho} + h_u \, \rho_0 = \rho_0 h_0 \tag{4}$$

The system of two equations (3) and (4) can be solved for h_c and h_u :

$$h_c = \frac{w\,\rho_0}{\hat{\rho} - \rho_0} \tag{5}$$

$$h_u = h_0 + \frac{w\,h_0}{\hat{h} - h_0} \tag{6}$$

where use of equation (2) was made to simplify the expressions.

The additional mass at time t after impact is:

$$\Delta m = \frac{\rho_0 h_0 w}{h_0 - \hat{h}} = \rho_0 \frac{w}{c} \tag{7}$$

where c:

$$c = \frac{h_0 - \hat{h}}{h_0} \tag{8}$$

4. MECHANISM OF DEFORMATION

The same basic assumptions as made in the report (1989) are used here, mainly:

1. The displacement in the radial direction r is negligible.
2. Only normal impact is considered.
3. The projectile remains in contact with the plate after impact.

The region of the plate in contact with the projectile of radius a is taken to be in regime D with respect to the bending forces and in regime 1 with respect to the membrane forces. The

annular region limited by the radius of the projectile, a, and the radius of the region unaffected by the impact at time t, $r_1(t)$, is considered in regime D-E for bending and in regime 1-2 for membrane action.

It follows that:

$$M_r(r,t) = M_\theta(r,t) = -M_0 , N_r(r,t) = N_\theta(r,t) = N_0 \ , \text{ for } 0 \le r \le a \tag{9}$$

$$\left.\begin{array}{l} -M_0 \le M_r(r,t) \le 0 , M_\theta(r,t) = -M_0 \\ 0 \le N_r(r,t) \le N_0 , N_\theta(r,t) = N_0 \end{array}\right\} \text{ for } a \le r \le r_1(t) ; \tag{10}$$

and for the region $r_1(t) \le r$:

$$M_r(r,t) = M_\theta(r,t) = N_r(r,t) = N_\theta(r,t) = Q(r,t) = 0 \tag{11}$$

The associated flow rules for regime D and D-E are:

$$\textit{regime} \begin{cases} D: & \dot{\kappa}_r , \dot{\kappa}_\theta \le 0 & (12) \\ D-E: & \dot{\kappa}_\theta \le 0 , \dot{\kappa}_r = 0 & (13) \end{cases}$$

where $\dot{\kappa}_r = -\dfrac{\partial^2 \dot{w}(r,t)}{\partial r^2}$ and $\dot{\kappa}_\theta = -\dfrac{1}{r}\dfrac{\partial \dot{w}(r,t)}{\partial r}$ are the radial and circumferential curvature rates of the deformed plate, respectively. The dot refers to differentiation with respect to the time t and the $(\,)'$ to differentiation with respect to r.

At time $t = 0^-$, the plate is flat and $w(r,0) = 0$. After impact, the projectile and the portion of the plate in contact with it move at the same velocity $v(0^+)$, $t = 0^-$ and $t = 0^+$ referring to the instant of time immediately before and immediately after impact.

Using the associated flow rule and satisfying the continuity conditions at $r = a$ and $r = r_1(t)$, the velocity field $\dot{w}$ can be shown to be given by the following relations:

$$\dot{w}(r,t) = \begin{cases} v(t), & 0 \le r \le a ; \\ v(t)\dfrac{r - r_1(t)}{a - r_1(t)} & a \le r \le r_1(t) ; \\ 0 , & r_1(t) \le r ; \end{cases} \tag{14}$$

Using the yield condition for plastic regime D in the moment equilibrium equation for the region $0 \leq r \leq a$:

$$(r M_r)' - M_\theta = r Q(r,t) \tag{15}$$

yields the shear $Q(r,t)$:

$$Q(r,t) = 0 \text{ for } 0 \leq r \leq a \tag{16}$$

The equation of motion in the x_3-direction for the region in contact with the projectile results in:

$$\left(M_p + \mu \pi a^2\right) \dot{w}(a,t) = -\frac{\rho_0 \pi a^2}{c} \left(\dot{w}^2(a,t) + w(a,t)\dot{w}(a,t)\right) - q_0 \pi a^2$$

$$- 2\pi a N_0 \frac{-w'(a,t)}{1 + \frac{w'^2(a,t)}{2}} \tag{17}$$

The integration of the velocity field (14) over the time domain for the region $a \leq r \leq r_1(t)$ gives the plate deflection $w(r,t)$:

$$w(r,t) = \int_0^t v(t) \frac{r - r_1(t)}{a - r_1(t)} dt \tag{18}$$

It can be concluded from equation (14) that the slope $w'(r,t)$ for the annular region is independent of r:

$$w'(r,t) = \int_0^t \frac{v(t)}{a - r_1(t)} dt \tag{19}$$

the acceleration field $\dot{w}(r,t)$ for the outside affected area is given by:

$$\dot{w}(r,t) = \dot{v}(t) \frac{r - r_1(t)}{a - r_1(t)} + v(t) \frac{\dot{r}_1(t)(r-a)}{(a - r_1(t))^2} \tag{20}$$

Similarly, the equilibrium equation governing the behavior of the region $a \leq r \leq r_1(t)$ in the direction of impact is:

$$2\pi a N_0 \frac{-w'(a,t)}{1+\frac{w'^2(a,t)}{2}} = q_0\pi(r_1^2(t)-a^2) + \frac{d}{dt}\left\{\int_a^{r_1(t)} 2\pi\mu r\dot{w}(r,t)\,dr\right\}$$

$$+ \frac{d}{dt}\left\{\int_a^{r_1(t)} 2\pi\frac{\rho_0}{c} r\,w(r,t)\dot{w}(r,t)\,dr\right\} \qquad (21)$$

Successive integration of the quantities in the right hand side of the previous equation need to be done in order to get a simpler expression for use in the numerical scheme. The first integral yields:

$$\frac{d}{dt}\left\{\int_a^{r_1(t)} 2\pi\mu r\dot{w}(r,t)\,dr\right\} = 2\pi\mu\left[\frac{\dot{v}(t)}{a-r_1(t)}\left(\frac{r_1^3(t)-a^3}{3} - r_1(t)\frac{r_1^2(t)-a^2}{2}\right)\right.$$

(22)

$$\left. + \frac{v(t)\dot{r}_1(t)}{(a-r_1(t))^2}\left(\frac{r_1^3(t)-a^3}{3} - a\frac{r_1^2(t)-a^2}{2}\right)\right]$$

The evaluation of the second integral results in:

$$\frac{d}{dt}\left\{\int_a^{r_1(t)} 2\pi\frac{\rho_0}{c} r\,w(r,t)\dot{w}(r,t)\,dr\right\} = 2\pi\frac{\rho_0}{c}\int_a^{r_1(t)} \dot{w}^2(r,t)\,r\,dr$$

$$+ 2\pi\frac{\rho_0}{c}\int_a^{r_1(t)} w(r,t)\ddot{w}(r,t)\,r\,dr \qquad (23)$$

where:

$$\int_a^{r_1(t)} \dot{w}^2(r,t)\, r\, dr = \frac{v^2(t)}{12}(r_1(t)-a)(r_1(t)+3a) \tag{24}$$

and using integration by parts and the fact that $w'(r,t)$ is independent of r, the following result is deduced:

$$\int_a^{r_1(t)} r\, w(r,t)\ddot{w}(r,t)\,dr = w(r_1(t)) \int_a^{r_1(t)} r\,\ddot{w}(r,t)\,dr - \int_a^{r_1(t)} w'(r,t) \left(\int_a^r \ddot{w}(s,t)\, s\, ds \right) dr \tag{25}$$

Substitution of (22) to (25) in the equilibrium equation (21) results in:

$$2\pi a N_0 \frac{-w'(a,t)}{1+\frac{w'^2(a,t)}{2}} - q_0\pi(r_f^2(t)-a^2) = rhs1(r,t) + rhs2(r,t) + rhs3(r,t) + rhs4(r,t) \tag{26}$$

where:

$$rhs1(r,t) = \frac{\pi\mu}{3}\dot{v}(t)(r_1^2(t)+a\,r_1(t)-2a^2) + \frac{\pi\mu}{3}v(t)\dot{r}_1(t)(a+2r_1(t)) \tag{26.1}$$

$$rhs2(r,t) = \pi\frac{\rho_0}{c}\frac{v^2(t)}{6}(r_1(t)-a)(r_1(t)+3a) \tag{26.2}$$

$$rhs3(r,t) = \Big[\dot{v}(t)\,(r_1^2(t) + a\,r_1(t) - 2a^2) + v(t)\dot{r}_1(t)\,(a + 2r_1(t)) \Big] \pi \frac{\rho_0}{c} \frac{w(r_1(t),t)}{3} \tag{26.3}$$

$$rhs4(r,t) = -\Big[\dot{v}(t)\,(3a^3 - 5a^2 r_1(t) + a\,r_1^2(t) + r_1^3(t)) + v(t)\dot{r}_1(t)\,(r_1^2(t) - a^2) \Big] \frac{\pi \rho_0}{6c} w'(r,t) \tag{26.4}$$

Equations (17) and (26) are the governing equations for $v(t)$ and $r_1(t)$. From these variables, one can deduct the force-moment fields and the deflection field.

The numerical solution of these equations in time is possible only if the values of $r_1(0^+)$, $\dot{r}_1(0^+)$, $v(0^+)$ and $\dot{v}(0^+)$ are known. These are obtained from the following equations.

Equations (17) and (26) evaluated at time $t = 0^+$ result in:

$$(M_p + \mu\pi a^2)\,\dot{v}(0^+) + \frac{\rho_0}{c}\pi a^2 v^2(0^+) = -q_0 \pi a^2 \tag{27}$$

$$-q_0 \pi (r_1^2(0^+) - a^2) = rhs\,(r_1(0^+),0^+) \tag{28}$$

where:

$$rhs\,(r_1(0^+),0^+) = \frac{\mu\pi}{3}\Big[v(0^+)(r_1^2(0^+) + a\,r_1(0^+) - 2a^2) + v(0^+)\dot{r}_1(0^+)(a + 2r_1(0^+)) \Big] + \pi \frac{\rho_0}{c} \frac{v^2(0^+)}{6} (r_1(0^+) - a)(r_1(0^+) + 3a) \tag{28.1}$$

The conservation of linear momentum over the time interval immediately before and immediately after impact gives:

$$M_p\, v(0^-) = M_p\, v(0^+) + \mu\, \pi\, a^2\, v(0^+) + \int_a^{r_1(0^+)} 2\,\pi\,\mu\,\dot{w}(r,0^+)\, r\, dr \tag{29}$$

where $v(0^-)$ is the impact velocity of the projectile immediately before impact.

Equation (29) can be simplified to yield:

$$M_p\, v(0^-) = (M_p + \mu\,\pi\, a^2)\, v(0^+) + \mu\,\frac{\pi}{3} v(0^+)\,(r_1(0^+)^2 - 2a^2 + a\, r_1(0^+)) \tag{30}$$

The moment equilibrium equation for the region $a \le r \le r_1(t)$ at $t = 0^+$ yields:

$$(r\, M_r)' - M_\theta = -\int_a^r \left(-q_0 - \mu\,\ddot{w}(r,0^+) \right) r\, dr \tag{31}$$

Using the yield relation for regime D-E, the continuity condition at $r = r_1(t)$, ($M_r = 0$), and the above equation gives:

$$\begin{aligned} M_0 r_1(0^+) = {} & \frac{q_0}{6}(r_1(0^+) - a)^2 (r_1(0^+) + 2a) \\ & + \mu\,\frac{\dot{v}(0^+)}{12}(r_1(0^+) - a)^2 (r_1(0^+) + 3a) \\ & + \mu\, v(0^+)\,\frac{\dot{r}_1(0^+)}{12}(r_1(0^+) - a)(r_1(0^+) + a) \end{aligned} \tag{32}$$

These four equations (Equations 27, 28, 30 and 32), can be combined to give an eighth degree polynomial equation for $r_1(0^+)$:

$$\sum_{i=0}^{i=8} A_i\, r_1{}^i(0^+) = 0 \tag{33}$$

where A_i are functions of the material properties of the plate and honeycomb, the properties of the hitting projectile and its velocity before impact.

Once $r_1(0^+)$ is determined, $v(0^+)$, $\dot{v}(0^+)$ and $\dot{r}_1(0^+)$ can be calculated from the system of four equations.

5. NUMERICAL METHOD

The equations of equilibrium (17) and (26) are integro-differential equations and both the deflection and the acceleration have to be calculated numerically from the velocity.

A forward Euler method is used to evaluate the acceleration from $v(t)$ and the rate of variation of the radius of the affected region with time, $\dot{r}_1(t)$, from $r_1(t)$:

$$\dot{v}_{num}(t_i) = \frac{v_{i+1} - v_i}{\Delta t} \tag{34}$$

$$\dot{r}_{1num}(t_i) = \frac{r_{1i+1} - r_{1i}}{\Delta t} \tag{35}$$

where Δt is the time step in the numerical scheme and t_i, v_i and r_{1i} are:

$$t_i = i\,\Delta t \tag{35.1}$$

$$v_i = v(t_i) \tag{35.2}$$

$$r_{1i} = r_1(t_i) \tag{35.3}$$

The trapezoidal rule gives a good estimate of the deflection $w(r,t)$ and the slope $w'(r,t)$ from the velocity field $\dot{w}(r,t)$:

$$w_{num}(r,t_i) = \frac{\Delta t}{2}\left[v(0)\frac{r - r_1(0)}{a - r_1(0)} + 2v(t_1)\frac{r - r_1(t_1)}{a - r_1(t_1)} + \cdots\right.$$

$$\left. + 2v(t_{i-1})\frac{r - r_1(t_{i-1})}{a - r_1(t_{i-1})} + v(t_i)\frac{r - r_1(t_i)}{a - r_1(t_i)}\right] \tag{36}$$

$$w'_{num}(r, t_i) = \frac{\Delta t}{2}\left[\frac{v(0)}{a - r_1(0)} + 2\frac{v(t_1)}{a - r_1(t_1)} + \cdots\right.$$

$$\left. + 2\frac{v(t_{i-1})}{a - r_1(t_{i-1})} + \frac{v(t_i)}{a - r_1(t_i)}\right] \tag{37}$$

Replacing these quantities in the equations of motion results in a system of two equations with two unknowns, v_{i+1} and r_{1i+1}.

The integration of the deflection at a particular point given by $a < r$ at time t has to be done during the time intervals when the point is in the region affected by the motion.

6. DISCUSSION OF THE RESULTS

Several experiments involving the impact of a projectile on a sandwich plate were conducted at the impact laboratory at the University of California at Berkeley. The setup of the tests and the collection of data are discussed in detail in Beckmann (1990).

Using the properties of each of seven typical tests, the herein proposed method was used to predict certain quantities that were also measured in experiments. The velocity of the projectile, the thickness of the Aluminum plate, the type of honeycomb NOMEX core used in the sandwich plate and its crush strength are presented in table 1 for each of seven tests.

In order to compare the results, certain quantities which include the velocity of the projectile immediately after impact, the initial radius of the affected region, the final radius of this region, the total time of contact and the final deflection were predicted using the proposed method. In a first approximation, the mass of the accumulating honeycomb was neglected. Then it was included to see what effect it has on the general behavior. The results are presented in table 2.

As can be expected, the velocity immediately after impact is smaller when the crushed honeycomb mass is included. The difference in the total time of contact is negligible. The initial and final radius of the region affected by the motion are greater when the mass is included. This result is due to the fact that the plate stiffens once the mass of the crushed core is added. Thus a bigger region

plastifies.

Comparison between the experimental results and the predicted ones are included in table 3, where t_f is total the contact time, $r_1(t_f)$ and $w(0,t_f)$ the corresponding radius of the affected region and the central deflection. The results are in good agreement with the quantities measured from the dynamic impact tests.

Table 1- Experimental Data.

Experiment Designation	Hexcel Core Type	Al Plate Thick.(mm)	Crush Strength $q_0\ (n/m^2)$	Impact Velocity $v\ (0^-)\ (m/s)$
1	1/4-0.001	0.8128	668795.0	19.35
2	1/4-0.001	1.27	668795.0	19.28
3	1/8-0.001	1.27	1889175.0	24.21
4	1/8-0.002	0.8128	5722684.0	34.01
5	1/8-0.002	1.27	5722684.0	34.21
6	1/8-0.001	1.27	1889175.0	26.47
7	1/8-0.001	1.27	1889175.0	28.27

Table 2- Predicted Results Including and Neglecting Accumulated Honeycomb Mass

Exp.	t_f (ms)		$w(0,t_f)$ (cm)		$r(t_f)$ (cm)		$v(0^+)$		$r_1(0^+)$	
Num.	Inc.	Excl.	Inc.	Excl.	Inc.	Excl.	Inc.	Excl.	Inc.	Excl.
1	125	125	1.349	1.353	8.765	8.737	19.026	19.027	5.456	5.441
2	108	108	1.160	1.162	9.590	9.559	18.626	18.629	6.652	6.627
3	80	80	1.047	1.051	7.207	7.182	23.589	23.592	5.325	5.307
4	66	66	1.157	1.165	5.077	5.048	33.582	33.583	4.223	4.215
5	57	57	1.028	1.035	5.565	5.547	33.484	33.487	4.572	4.558
6	83	85	1.197	1.202	7.378	7.348	25.792	25.795	5.328	5.307
7	86	86	1.322	1.327	7.505	7.471	27.549	27.553	5.331	5.307

Table 3- Comparison of Predicted Value with Data

Experiment Designation	t_f (ms)		$w(0,t_f)$ (cm)		$r(t_f)$ (cm)	
	Exp.	Pred.	Exp.	Pred.	Exp.	Pred.
1	160	125	1.23	1.35	9.14	8.77
2	152	108	1.06	1.16	10.54	9.59
3	106	80	0.93	1.05	7.23	7.21
4	84	66	1.25	1.16	4.83	5.08
5	92	57	1.14	1.03	5.27	5.56
6	112	83	1.08	1.20	7.74	7.38
7	122	86	1.22	1.32	7.87	7.50

APPENDIX D

REFERENCES

1. Lee, E. H., and Mallett, R. L., Structural Analysis and Design for Energy Absorption and Impact. Final Report. Washington, D. C., U. S. Dept. of Transportation, DOT-TST-76-44, December, 1975.

2. Perrone, N., "Biomechanical and Structural Aspects of Design for Vehicle Impact." In: Human Body Dynamics: Impact, Occupational and Athletic Aspects, ed. by D. N. Ghista. Oxford, Clarendon Press, p. 181, 1982.

3. Stronge, W. J., and Shim, V. P.-W., "Lateral Crushing in Tightly Packed Arrays of Thin-Walled Metal Tubes," Int. J. Mech. Sci, v. 28, pp. 709-728, 1986.

4. Johnson, W., and Mamalis, A. G., Crashworthiness of Vehicles. Mechanical Engineering Publications, Inst. of Mech. Engrs., London, 1978.

5. Jones, N., and Wierzbicki, T., eds. Structural Crashworthiness. London, Butterworth, 1983.

6. Paul, L. S., Identification of Superior Energy-Absorbing Materials for School Bus Interiors. Final Report. v. 1 and 2. ASL Engineering, Santa Barbara, CA. U. S. Dept. of Transportation, DOT RS 805-270 and 805-271, 1980.

7. Fay, R., and Kaplan, M. A., "Energy Absorbing Corrugated Metal Highway Safety Barrier." Highway Research Record, No.460, pp. 20-29, 1973.

8. Carney, J. F. III, and Sazinski, R. J., "Portable Energy Absorbing System for Highway Service Vehicles," ASCE Transp. Eng. J., v. 104, No. TE4, 1978.

9. Transportation Research Board (U.S.) Vehicle Barrier Systems. TRB Record 566, 1976.

10. Cronkhite, J. D., Berry, V. L., and Winter, R., Investigation of the Crash Impact Characteristics of Helicopter Composite Structures. Applied Technology Laboratories, U. S. Army Research and Technology Labs., Fort Eustis, VA, USA AVARADCOM, TR-82-D-14, 1983.

11. Highway Research Board. Design of Traffic Safety Barriers. 1971, No. 343, and Development of Safer Roadside Structures and Protective Systems, 1969, No. 259.

12. Bekos, J. D., Scale Model Study of Low Density Concrete Impact Attenuators. Ohio Dept. of Transportation. U. S. Dept. of Transportation, DOT-02-77, 1978.

13. Cronkhite, J. D., "Helicopter Structural Crashworthiness." In: Symposium on Vehicle Crashworthiness including Impact Biomechanics, ed. by P. Tong et al. New York, ASME, AMD 79, pp. 57-73, 1986.

14. Foye, H. L., Swindelhurst, C. W., and Hodges, W. T., "Crashworthiness Test for Composite Fuselage Structure." In: Fibrous Composites in Structural Design. New York, Plenum Press, pp. 241-257, 1980.

15. Sayir, M., and Koller, M. G., "Dynamic Behavior of Sandwich Plates," J. appl. Math. and Phys. (ZAMP), v. 37, pp. 78-130, 1986.

16. Plantima, F. J., Sandwich Construction. New York, J. Wiley, 1966.

17. Green, A. E., and Naghdi, P. M., "A Theory of Laminated Composite Plates," IMA J. appl. Math., v. 29, p. 123, 1982.

18. Yu, Y. Y, "A New Theory of Elastic Sandwich Plates -- One-dimensional Case," J. appl. Mech., v. 26, pp. 415-421, 1959.

19. Koller, M. G., "Elastic Impact of Spheres on Sandwich Plates," ZAMP, v./ 37, pp. 256-269, 1986.

20. Vinson, J. R., "Optimum Design of Composite Honeycomb Sandwich Panels Subjected to Uniaxial Compression," AIAA J., v. 24, pp. 1690-1696, 1986.

21. Herrmann, W., "Constitutive Equations for Dynamic Computations of Ductile Porous Material," J. appl. Phys., v. 40, p. 2490, 1969.

22. Goldsmith, W., and Kabo, J. M., "Performance of Baseball Caps, Am. J. Sports Medicine, v. 10, pp. 31-37, 1982.

23. Abramowicz, A. "The Effective Crushing Distance in Axially Compressed Thin-Walled Columns," Int. J. Impact Engng., v. 1, pp. 309-317, 1983.

24. Abramowicz, A., and Jones, N., "Dynamic Axial Crushing of Circular Tubes," Int. J. Impact Engng., v. 2, pp. 263-282, 1984.

25. Abramowicz, A., and Wierzbicki, T., "Axial Crushing of Foam-Filled Tubes," Int. J. Mech. Sci., v. 30, pp. 263-271, 1988.

26. Alexander, J. M., "An Approximate Analysis of the Collapse of Thin Cylindrical Shells under Axial Loading," Q. J. Mech. appl. Math., v. 13, pp. 10-15, 1960.

27. Ezra, A. A., and Fay, R. J., "An Assessment of Energy Absorbing Devices for Prospective Use in Aircraft Impact Situations." In: Dynamic Response of Structures, ed. by G. Hermann and N. Perrone. Oxford, Pergamon Press, pp. 225-246, 1972.

28. Gary, G., "Dynamic Buckling of an Elasto-Plastic Column," Int. J. Impact Engng., v. 1, pp. 357-375, 1983.

29. Hull, D., "Axial Crushing of Fiber-Reinforced Composite Tubes." In: Structural Crashworthiness, ed. by N. Jones and T. Wierzbicki. London, Butterworths, pp. 118-135, 1963.

30. Johnson, W., and Reid, S. R., "Metallic Energy Dissipating Systems," Appl. Mech. Rev., v. 31, pp. 277-288, 1978.

31. Jones, N., and Abramowicz, A., "Static and Dynamic Axial Crushing of Circular and Square Tubes." In: Metal Forming and Impact Mechanics, ed. by S. R. Reid. Oxford, Pergamon Press, pp. 225-247, 1985.

32. Klintworth, K. W., and Stronge, W. J., "Elasto-plastic Yield Limits and Deformation Laws for Transversely Crushed Honeycombs," Int. J. Mech. Sci., v. 30, pp. 273-292, 1988.

33. Mamalis, A. G., and Johnson, W., "The Quasi-Static Crumpling of Thin Wall Circular Cylinders and Frustra under Axial Compression, Int. J. Mech. Sci., v. 25, pp. 713-732, 1983.

34. Mamalis, A. G., Johnson, and Viegelahn, G. L., "The Crumpling of Steel Thin-Walled Tubes and Frustra under Axial Compression at Elevated Strain Rates -- Some Experimental Results," Int. J. Mech. Sci., v. 26, pp. 537-548, 1984.

35. Mamalis, A. G., et al., "The Inextensible Collapse of Grooved Thin-Wall Cylinders of PVC under Axial Loading," Int. J. Impact Engng., v. 4, pp. 41-56, 1986.

36. Mamalis, A. G., et al., "On the Inextensible Axial Collapse of Thin PVC Conical Shells," Int. J. Mech. Sci., v. 28, pp. 323-335, 1986.

37. Mamalis, A. G., et al., "Extensible Plastic Collapse of Thin-Wall Frustra as Energy Absorbers," Int. J. Mech. Sci., v. 28, pp. 219-230, 1986.

38. Reddy, T. Y., and Wall, R. J., "Axial Compression of Foam-Filled Thin-Walled Circular Tubes," Int. J. Impact Engng., v. 7, pp. 151-166, 1988.

39. Reid, S. R., "Metal Tubes as Impact Energy Absorbers." In: Metal Forming and Impact Mechanics, ed. by S. R. Reid. Oxford, Pergamon Press, pp. 249-269, 1985.

40. Reid, S. R., and Reddy, T. Y., "Static and Dynamic Crushing of Tapered Sheet Metal Tubes," Int. J. Mech. Sci., v. 28, pp. 628-638, 1986.

41. Reid, S. R., and Reddy, T. Y., "Axial Crushing of Foam-Filled Tapered Sheet Metal Tubes," Int. J. Mech. Sci., v. 28, pp. 643-656, 1986.

42. Reid, S. R., Reddy, T. Y., and Gray, M. D., "Static and Dynamic Axial Crushing of Foam-Filled Sheet Metal Tubes," Int. J. Mech. Sci., v. 28, pp. 295-322, 1986.

43. Shim, V. P., and Stronge, W. J., "Lateral Crushing of Thin-Walled Tubes between Cylindrical Indenters," Int. J. Mech. Sci., v. 28, pp. 683-707, 1986.

44. Shim, V. P., and Stronge, W. J., "Lateral Crushing in Tightly Packed Arrays of Thin-Walled Metal Tubes," Int. J. Mech. Sci., v. 28, pp. 708-728, 1986.

45. Stronge, W. J., "Impact and Perforation of Cylindrical Shells by Blunt Missiles," In: Metal Forming and Impact Mechanics, ed. by S. R. Reid. Oxford, Pergamon Press, pp. 289-302, 1985.

46. Stronge, W. J., and Shim, V. P. W., "Dynamic Crushing of a Ductile Cellular Array," Int. J. Mech. Sci., v. 29, pp. 381-400, 1987.

47. Thornton, P. H., Mahmood, H. E., and Magee, C. L., "Energy Absorption in Structural Collapse." In: Structural Crashworthiness, ed. by N. Jones and T. Wierzbicki. London, Butterworths, pp. 96-117, 1983.

48. Veillette, J. R., and Carney, J. F. III, "Collapse of Braced Tubes under Impact Load," Int. J. Impact Engng., v. 7, pp. 126-138, 1988.

49. Wang, R., Han, M., Huang, Z., and Yan, Q., "An Experimental Study of Dynamic Axial Plastic Buckling of Cylindrical Shells," Int. J. Impact Engng., v. 1, pp. 249-256, 1983.

50. Wierzbicki, T., "Crushing Analysis of Metal Honeycombs," Int. J. Impact Engng., v. 1, pp. 157-176, 1983.

51. Wierzbicki, T., and Shat, S. W., "A Moving Hinge Solution for Axisymmetric Crushing of Tubes," Int. J. Mech. Sci., v. 28, pp. 135-151, 1986.

52. Bernard, M. L., and Lagace, P. A., "Impact Resistance of Composite Sandwich Plates, J. Reinforced Plastics and Composites, v. 8, pp. 432-445, 1989.

53. Corbett, G. G., Resid, S. R., and Alhassani, S. T. S., "Resistance of Steel Concrete Sandwich Tubes to Penetration," Int. J. Impact Engng., v. 9, pp. 191-203, 1990.

54. Hsueh, D. W., "Normal Perforation of a thin Infinite Plate by a Flat-Headed Cylindrical Projectiles, Int. J. Impact Engng., v. 8, pp. 133-139, 1989.

55. Wang, C. Y., and Yew, C. H., "Impact Damage in Composite Laminates," Computers and Structures, v. 37, pp. 967-982, 1990.

56. Rechak, S., and Sun, C. T., "Optimal Use of Adhesive Layers in Reducing Impact Damage in Composite Laminates," J. Reinforced Plastics and Composites, v. 0, pp. 569-582, 1990.

57. Lin, H. J., and Lee, Y. J., "Use of Statical Indentation Laws in the Impact Analysis of Composite Laminated Plates and Shells,, J. appl. Mech., Trans. ASME, v.57, pp. 787-789, 1990.

58. Akimune, Y., "Impact Damage and Strength Degradation in a Silicon Carbide Reinforced Silicon Nitride Composite," J. Amer. Ceramic Soc., v. 73, pp. 3019-3025, 1990.

59. Kau, H. T., "A study of the Impact Behavior of Chopped Fiber Reinforced Composite," Polymer Composites, v. 11, pp. 253-264, 1990.

60. Elzein, M. S., and Reifsnider, K. L., "On the Prediction of Tensile Strength after Impact of Composite Laminates," J. Composites Technology and Research, v. 12, pp. 147-154, 1990.

61. Christoforou, A. P., and Swanson, S. R., "Analysis of Impact Response of Composite Plates," Int. J. Solids Structures,, v. 27, pp. 161-170, 1991.

62. Qian, Y., and Swanson, S. R., "A comparison of Solution Techniques for Impact Response of Composite Plates," Composite Structures, v. 14, pp. 177-192, 1990.

63. Lin, H. J., and Lee, Y. J., "On the Inelastic Impact of Composite Laminated Plate and Shell Structures," Composite Structures, v. 14, pp. 89-111, 1990.

64. Evans, K. E., "The Design of Doubly Curved Sandwich Panels with Honeycomb Cores," Composite Structures, v/ 17, 95-11, 1990.

65. Akay, M., andanna, R. "A Comparison of Honeycomb-Core and Foam-Core Carbon-Fibre Epoxy Sandwich Panels," Composites, v. 21, pp. 325-331, 1990.

66. Wittenauer, J., and Norris, B., "Structural Honeycomb Materials for Advanced Aerospace Designs,"JOM--J. Minerals Metals & Materials Soc., v. 42, pp. 36-41, 1990.

67. Ding, Y. L., "Optimum Design of Honeycomb Sandwich Constructions with Buckling Constraints," Computers Structures, v. 33, pp. 1255-1264, 1989.

68. Klintworth, J. W., and Stronge, W. J., "Plane Punch Indentation of a Ductile Honeycomb," Int. J. Mech. Sci., v. 31, pp. 359-378, 1989.

69. Zhang, S. Y., Tsai, L. W., and Liu, J. Q., "Strain Energy Density Ratio Criterion for Fracture of Composite Materials," Engng. Fracture Mechanics, v. 37, pp. 881-889, 1990.

70. Kumar, P., and Narayanan, M. D., "Energy Dissipation of Projectile Impacted Panels of Glass Fabric Reinforced Composite," Composite Structures, v. 15, pp. 75-90, 1990.

71. Rmili, M., Rouby, D., Fantozzi, G., and Lamico, P., "Energy Toughness Parameters for a 2d Carbon Fibre Reinforced Carbon Composite," Composites, Science and Technology, v. 37, pp. 207-221, 1990.

80. Nairn, J. A., "The Strain Energy Release Rate of Composite Microcracking -- a Variational Approach," J. Composite Materials, v. 23, pp. 1106-1129, 1989.

81. Lin, H. J., and Lee, Y. J., "On the Inelastic Impact of Composite Laminated Plate and Shell Structures," Composite Structures, v. 14, pp. 89-111, 1990.

&1L

APPENDIX E

TABLE 1

STATIC TEST RESULTS ON SANDWICH SPECIMENS
Original Core Thickness of the 5052 Aluminum Hexcel : 0.75 in
Facing Material: 5052 H32 Aluminum

Run No.	Composition		Full Crush Conditions				Punch Initiation	
	Core	Face Plate Thickness, in	Displacement, in[1]	%[2]	Avg. Press. psi	Energy Absorbed, in-lb	Displacement, in	Energy Absorbed, in-lb
1S[3]	1/8-.001	0.050[b]	≈0.54	≈71	640	≈2270	0.36	1620
2S	1/8-.001	0.032[a]	0.51	67	550	1820	0.38	1440
3S[4]	1/4-.001	0.050[b]	0.60	80	410	1590	0.42	890
4S[4]	1/4-.001	0.032[b]	0.62	88	380	1630	0.55	12605S
5S	1/8-.002	0.032[a]	0.48	64	990	3140	0.22	1450
6S	1/8-.002	0.050[a]	0.45	60	1130	3320	0.23	1790

[1] "Full" crush represents the condition where load-displacement curve rises denoting densification (does not occur at the same displacement as for cores alone).

[2] % thickness decrease = (change in thickness)/(original core thickness) x 100

[3] Test No. 1S was stopped just short of full crush; values given at full crush are approximate.

[4] Edge effects were present in these tests. Creasing became visible at 0.40 in crush in Test 3S and at 0.53 in crush in Test 4S. Creasing started before punching.

[a] Top face plate completely punched through.

[b] Top face plate partially punched through.

TABLE 2
DYNAMIC TEST RESULTS ON SANDWICH SPECIMENS
Original Core Thickness of the 5052 Aluminum Hexcel: 0.75 in
Facing Material: 5052 H32 Aluminum

Run No.	Composition Core	Face Plate Thickness, in	Velocity, in/s Impact	Rebound	Momentum Balance,[1] %	Crush[2] %	Avg. Press. psi	Contact Time, ms
1D	1/4-.001[c]	0.032	762	-151	+2.6	64.2	422	1.6
2D	1/4-.001[c]	0.050	759	-209	-1.4	55.1	501	1.52
3D	1/8-.001[b]	0.050	953	-172	+3.5	49.1	940	1.06
4D	1/8-.002[a]	0.032	1339	-53	+1.6	65.1	1240	0.84
5D	1/8-.002[a]	0.050	1347	-50	+1.2	59.8	1540	0.92
6D	1/8-.001[b]	0.050	1042	-201	+0.1	57.2	980	1.12
7D	1/8-.001[b]	0.050	1113	-202	-2.6	64.3	978	1.22

Run No.	Energy Absorbed, in-lb Total	Per Inch of Crush	Per % of Crush	Indentation Diameter, in
1D	1370	2820	21.3	7.2
2D	1270	3045	23.0	8.3
3D	2160	5890	44.0	5.7
4D	4040	8240	62.0	3.8
5D	4080	9070	68.2	4.15
6D	2350	5500	41.1	6.1
7D	2670	5560	41.5	6.2

[1] Momentum balance = (change in momentum)/(initial momentum of projectile)x100
Change in momentum = initial projectile momentum - (pendulum momentum + rebound projectile momentum)

[2] Crush = (change in thickness of sample)/(initial core thickness) x 100

[a] Top face plate completely punched through

[b] Top face plate partly punched through. This condition was also previously found for the 1/8-.001-0.032 sandwich (Annual Report, 1989)

[c] Top face plate not punched through (no shear)